**AIAA PAPER
78-147**

Real Flow Limitations in Supersonic Airplane Design

R.M. Kulfan and A. Sigalla, *Boeing
Commercial Airplane, Co., Seattle, Wash.*

AIAA 16TH AEROSPACE SCIENCES MEETING

Huntsville, Alabama/January 16-18, 1978

REAL FLOW LIMITATIONS IN SUPERSONIC AIRPLANE DESIGN

R. M. Kulfan, Senior Specialist Engineer
A. Sigalla, Chief, Technology—Preliminary Design
Boeing Commercial Airplane Company, Seattle, Washington

Abstract

Experimental studies, including pressure measurements, force measurements and flow visualization techniques, have shown that predicted aerodynamic performance levels of supersonic wings can be achieved only when the flow remains attached over the entire wing surface.

The nature of the breakdown of potential flow on supersonic wings is discussed and illustrated with experimental flow visualization pictures and wind-tunnel data. Various types of flow breakdown are examined. Simplified flow analogies that explain these flow phenomena are developed. Practical procedures that ensure design for attached flow at prescribed conditions are described. Flow analogies are used to explore the impact of various airplane design parameters on the breakdown of attached flow.

1.0 Introduction

The design of efficient, very highly swept supersonic wings is one of the more difficult problems in aeronautics. These highly swept wings are of interest because they have the potential, according to theory, of having relatively low drag at supersonic lifting conditions.

Well known supersonic wing theory[1] indicates that the leading edge of a wing must be at an angle of sweepback greater than the angle weak shockwaves make with the free stream at corresponding Mach numbers to achieve low drag at lifting conditions. Sweepback angles of 70 to 75 degrees are necessary for Mach numbers in the range of 2.0 to 3.0 Theoretical predictions indicate that an airplane with a wing of such high sweep would have an advantage of approximately 15 to 20 percent in lift/drag ratio when compared to an airplane having a much lower sweepback angle (for example, 50 degrees).

When it was first attempted to substantiate these very encouraging predictions with wind-tunnel models, it was found that the experimental results did not confirm them at all. Subsequent examinations revealed that the low drag predicted by theory was not achieved because the flow pattern around the wings, implicit in theory, did not occur in practice. Viscosity, which normally has a relatively small effect on the overall flow over wings at normal cruise lift conditions, had a rather substantial effect on these highly swept wings.

Consider as an example a wing at Mach 3.0 and at an angle of attack of 4 degrees—typical supersonic conditions. With the wing swept 75 degrees to achieve low drag, the Mach number component normal to the leading edge is 0.78. Hence near the wing leading edge, a recognized subsonic flow condition is produced. The leading edge flow is governed by the angle normal to the leading edge. Using simple sweep theory, the normal angle of attack for this example is found to be approximately 15 degrees. Experience indicates that the airstream normally will not be able to flow around the leading edge at this large angle of attack without flow separation. This is particularly true for the thin airfoils that are characteristic of supersonic wing designs. This leading-edge flow separation completely alters the character of the flow pattern over the wing.

Leading-edge flow separation is only one of the reasons why the predicted low drag levels of highly swept wings could not be obtained. The flow over the wing, which is at a relatively low pressure, must adjust to free stream pressure through a shock wave at the trailing edge. If the theoretical flow requires too large a pressure rise, trailing-edge separation occurs. Again the flow pattern postulated by theory cannot occur and the theoretical drags cannot be achieved. Similar problems can occur on other parts of such a highly swept wing. The establishment of a flow consistent with theoretical low drag is, therefore, contingent on the response of the boundary layer to potentially severe conditions all over the wing. The development and behavior of highly swept wing boundary layers under complicated three-dimensional flow conditions is not amerable to theoretical calculations. Necessary wing design limitations cannot be defined strictly on the basis of analytical studies, and therefore had to be developed from experimental test programs.

This paper presents a comprehensive set of design conditions that can be used to define efficient, highly swept supersonic wings. If these conditions are applied as constraints to theoretical calculations, the flow pattern resulting from analysis would not have a very large effect on the wing boundary layers and the theoretical flow, and drag, could be expected to be obtained in practice.

The results presented in this paper are based on work that began in the late 1950s and was carried through the U.S. SST program until cancellation of the program in 1971. The object of the work was to develop methods for the design of efficient supersonic wings. More recently, interest in the design of such wings has been renewed both for eventual commercial[2] and military[3] applications. For the latter case, not only does the designer require low drag at cruising conditions, but he also requires a reasonable flow at higher lift coefficients associated with military maneuvers. A review of design methods to accomplish this is therefore timely and appropriate, and forms the subject of this paper.

In Section 2 the basic characteristics of supersonic wing planforms are discussed, pointing out the advantages of highly swept wings in supersonic flow. This is followed by a review of experimental results illustrating the basic flow problems of highly swept wings. The potential effects of warping the surface of such wings, (e.g., camber and twist) are discussed in

Section 3. The different possibilities of flow breakdown on highly swept, warped wings are discussed in Section 4, with emphasis on shockwave-induced separation. Constraints for the design of highly swept supersonic wings are presented in Section 5. In Section 6, these design constraints are used to explain the breakdown of attached flow on a number of wind-tunnel models. Successful design applications of these criteria are discussed in Section 7.

2.0 Aerodynamics of Highly Swept Wings

The aerodynamic efficiency of an airplane is characterized by its lift/drag ratio, L/D. The drag of a supersonic configuration typically consists of the skin friction drag, wave drag due to thickness, and drag due to lift. Supersonic drag due to lift includes both induced drag and wave drag due to lift. The theoretical drag polar (that is, the relationship between drag and lift) for any simple configuration can be expressed as:

$$C_D = C_{Do} + \frac{\alpha C_D}{\alpha C_L^2} \quad C_L^2$$

where C_{Do} is the drag coefficient at zero lift and is composed of both thickness wave drag and friction drag. $\alpha C_D/\alpha C_L^2$ is the drag-due-to-lift factor and is theoretically a constant.

The solution of this equation for maximum L/D gives the simple relation:

$$(L/D)_{max} = \frac{0.5}{\sqrt{C_{Do} (\alpha C_D/\alpha C_L^2)}}$$

Hence the attainment of high (L/D_{max}) is seen to depend on the two factors C_{Do} and $(\alpha C_D/\alpha C_L^2)$. The drag-due-to-lift factor is primarily affected by the wing selection. The friction drag is primarily determined by the Reynolds number and Mach number. The thickness wave drag is dependent on the wing shape and its thickness distribution.

Increased wing sweep so that the leading edge is behind the leading-edge shock (subsonic leading edge), as shown in Figure 1, is very beneficial in reducing both wave drag, C_{D_W}, and the drag-due-to-lift factor. Additional reductions in the drag-due-to-lift factor are indicated by carving out the less efficient aft area of a delta wing, thereby producing an "arrow" wing planform.

2.1 Highly Swept Wing Experimental Results

Results of wind-tunnel tests to substantiate the low drag levels of highly swept, supersonic wings are shown in Figures 2 and 3. The results indicate that the predicted zero lift drag levels are indeed achieved. However, the drag-due-to-lift factor is substantially higher than theoretical predictions, particularly when the leading edge is subsonic.

The wind-tunnel results[4,5] shown in Figure 3 associated the increased drag due to lift with a sudden change in the upper surface flow from an attached to a separated flow condition. The theoretical model and observed flow patterns are shown in Figure 4. The observed pattern was dominated by the formation of a leading-edge separation vortex characteristic of the flow pattern found on highly swept wings at subsonic speeds[6].

2.2 Flow Over a Highly Swept Wing

By virtue of extensive experimental and semi-empirical investigations,[7,8,9,10,11,12,13] the formation of the leading-edge separation vortex is well understood. For the subsonic leading-edge wing at angle of attack, the attachment line of the flow is back of the leading edge on the lower surface. There is, therefore, flow from the lower surface around the leading edge to the upper surface. The expansion of the flow going around the leading edge results in a very high negative pressure and a subsequent steep adverse pressure recovery gradient near the leading edge on the upper surface. The steep adverse pressure gradient can readily cause the three-dimensional boundary layer to separate from the surface. When separation occurs, the boundary layer leaves the wing surface along a swept separation line and rolls up into a region of concentrated vorticity which is swept back over the surface of the wing. The effect of this vortex is to alter the velocity distribution and hence the pressure distribution over the wing. The pressure distributions[14] in Figure 4 illustrate the effect of the leading-edge vortex on the upper surface. Note that the lower surface pressures are also affected. The lower surface effect is associated with the stagnation line moving to the leading edge when the leading-edge vortex is formed.

Typical pressure distributions and leading-edge vortex formation on two highly swept wings, with sharp and with round leading edge airfoils, are shown in Figure 5. The separation vortex springs from the entire leading edge of the sharp airfoil wing. The effect of the round leading edge is to reduce the adverse pressure gradient on the inboard portion of the wing. The leading edge separation starts near the wing tip and moves inboard with increasing angle of incidence. The formation of the leading-edge vortex affects the lift, pitching moment and drag on a highly swept wing[12]. The discussions in this paper are primarily concerned with the effect on drag. The theoretical drag force on a wing section as shown in Figure 6 is the resultant of a component of the surface normal force $(C_L\alpha)$, the thickness wave drag, friction drag, and a leading-edge thrust force, C_T. In practice the thrust force must develop from the large leading-edge pressure acting on the "nose" of the airfoil.

Experimental variations of the leading-edge thrust force obtained on a highly swept delta wing are compared with theoretical predictions in Figure 6 for two symmetrical (flat) wings and for a wing with conical camber. One of the two flat wings had a sharp leading-edge airfoil. The other flat wing and the wing with conical camber had rounded leading edges. Note that the flat wing loses the theoretically predicted thrust force at very low lift coefficients ($C_L \approx 0.05$). The rounded leading-edge airfoil is able to achieve a higher percentage of the leading-edge thrust force than the wing with a sharp airfoil. This loss

in leading-edge thrust force is directly associated with the formation of the leading-edge vortex. The conically cambered wing is able to achieve the predicted thrust force to a higher lift coefficient (C_L = .075). However, at negative lift coefficients, little if any leading-edge suction is achieved. This is discussed further in Section 3.

2.3 Leading-Edge Separation Criteria

It has been found experimentally that the nature of the flow over highly swept wings at incidence changes with increasing Mach number from a leading-edge separation type of flow to an attached flow over the upper surface of the wing[8]. On thin wings this can occur at a Mach number below that for which the leading edge is supersonic (i.e., the component of Mach number normal to the leading edge is less than 1).

In the analyses of separated flow around swept leading-edge wings it has been found useful to correlate the data in terms of conditions normal to the leading edge. The velocity components normal to the plane of the wing W_N, and normal to the leading edge of the wing in the plane of the wing, U_N, are:

$$W_N = U \sin \alpha$$

$$U_N = U \sin \alpha \cos \Lambda$$

The incidence angle normal to the leading edge, α_N, and the normal Mach number M_N are:

$$\alpha_N = \tan^{-1} (\tan \alpha / \cos \Lambda)$$

$$M_N = M \cos \Lambda \sqrt{1 + \sin^2 \alpha \tan^2 \Lambda}$$

As shown in Figure 7, the normal angle of incidence is appreciably higher than the wing angle of incidence α for a highly swept wing. Experimental correlations of flow over highly swept uncambered wings[8] have identified the boundary region shown in Figure 7 that separates the conditions (normal Mach number and normal incidence angles) for which attached flow, or leading-edge separation flow, exists. This boundary between separated and attached flow for uncambered wings can be approximated by the expression[16]:

$$M_N = 0.06 + 0.013 \alpha N$$

A round leading edge, as shown in Figure 7 and as previously discussed, tends to suppress the formation of separated flow to larger incidence angles relative to sharp leading-edge airfoils. The leading-edge vortex formation boundaries shown in Figure 8 have been constructed using the aforementioned sharp leading airfoil separation equation to illustrate the effect of wing leading-edge sweep. This separation criterion predicts the sudden formation of the leading-edge separation vortex on the flat wing model[4] shown in Figure 3.

As shown in Figure 9, this flat wing separation criterion can be applied to wings with varying leading-edge sweep by using the local leading-edge sweep angle[8].

To obtain the low drag potential of highly swept wings, leading-edge separation must be avoided. Otherwise the leading-edge thrust previously discussed cannot be achieved. Hence, the low drag-due-to-lift potential of swept flap wings appears to be unachievable for all but very low incidence angles.

3.0 Cambered and Twisted Wings

Properly designed warped wings can suppress the development of the leading-edge vortex and thereby shift the boundary for attached flow up to higher incidence angles (Figure 9).

The effect of wing camber and twist (wing warp) on suppressing the leading-edge separation is shown qualitatively in Figure 10. Wings designed to achieve a finite load distribution along the leading edge are cambered and twisted such that the leading edges of the wing align with the local flow direction. The attachment line lies along the leading edge. The expansion over the wing upper surface is greatly reduced, thereby eliminating the strong adverse pressure gradient near the leading edge. The thrust force on a cambered airfoil is achieved by action of the reduced expansion pressure on the relatively large "shoulder" area of the airfoil.

At angles of attack above or below the design incidence of a warped wing, the attachment line will move below or above the leading edge, respectively, and eventually may promote the formation of the separation vortex. At negative incidences, an adverse pressure gradient rapidly develops on the lower surface and quickly eliminates the leading-edge thrust force. The leading-edge thrust data shown in Figure 6 illustrate incidence effects on the chord force of a cambered wing.

Typical pressure distributions for warped and flat highly swept, supersonic wings are shown in Figure 11.

In addition to suppressing the formation of leading-edge separation, cambered wings offer low drag-due-to-lift potential. This low drag potential is only slightly less than the theoretical, but apparently unachievable, flat wing potential. A great deal of experimental and theoretical studies have been directed at developing low-drag cambered wings, and have achieved widely varying results. Some of the cambered wing designs, such as those shown in Figures 12 and 13, achieved significant aerodynamic improvements over comparable flat wings having the same planforms and thickness distributions. Others failed to show any improvement over flat wings. To further complicate matters, a successful camber wing design often would fail to achieve its low drag if airplane design parameters such as the wing thickness and/or design lift coefficient were increased, or if the body shape was altered.

The explanation came from flow visualization studies, which showed that the successful configurations had attached flow over the wing upper surface. Unsuccessful wings exhibited vortex dominated flow, strong shock and large regions of separated flow on the upper surfaces of the wings. Camber and twist design of a given configuration had to take into account, therefore, the influence of factors such as wing thickness, lift

coefficient, design pitching moment for low trim drag, and body shape. To make this possible, a more thorough understanding of the different types of flow in these wings became necessary, as discussed below.

4.0 Types of Flow on Highly Swept Wings

The unsuccessful cambered wings typically encountered strong spanwise flow near the trailing edge; flow separation behind a strong oblique shock near the wing leading edge; or separation behind a strong shock close to the trailing edge. The main types of flow observed on these highly swept, cambered, supersonic wings are shown in Figure 14. The attached flow corresponds to the theoretical conditions. The leading-edge vortex flow is characteristic of highly swept, flat wings. Often more than one of these conditions would exist simultaneously.

Figure 15 illustrates a typical breakdown of flow over a cambered wing design at Mach 3.0 as the angle of incidence is increased. Figure 16 illustrates how a change in mid-body contour can promote shock-induced flow separation. It is necessary to understand why flow breakdown can occur to enable the design of configurations that will be free from this undesirable condition. An approach that can lead to the successful design of supersonic airplanes is discussed below.

5.0 Cambered Wing Design Criteria

Careful examinations of test results have shown that the design of the wing camber and twist in conjunction with wing thickness and body effects must avoid (1) strong spanwise flow, (2) extremely high suction pressures, (3) inboard shock separation, and (4) trailing-edge shock separation.

Design criteria were needed to predict flow breakdown on the basis of potential flow analyses so that wing camber and twist could be developed or modified to avoid serious drag increases. In general, the type of flow over a wing depends on the combination of camber, twist, angle of attack, wing thickness distribution and airfoil shapes, body shape, and possible effects of other airplane components, and flight conditions. All of these contribute to the pressure distribution on the wing. The pressure distribution directly governs the nature of the flow over the wing.

The method that has been developed to help understand the flow phenomena involves the use of supersonic linear theory to estimate the pressure distribution on a wing. This pressure distribution is then examined to assess the probability of achieving the theoretical aerodynamic performance levels.

The recommended wing design approach is to design the camber and twist distribution to produce finite leading-edge pressures and mild pressure gradients. At the design conditions the nature of the flow is governed by wing upper surface pressure levels. Off-design conditions such as high maneuvering angles of attack may produce severe pressure gradients that result in boundary layer separation or the development of leading-edge vortices.

The design criteria considered here are those associated with pressure levels and were derived from a rather substantial body of experimental three-dimensional boundary layer separation results.

5.1 Avoiding High Suction Pressures

Linear theory estimates can provide theoretical negative pressures in excess of vacuum pressures. Experimental data[17,18,19] such as shown in Figure 17 indicate that it is advisable to reject theoretical solutions when predicted suction pressures exceed about 70 or 80 percent of vacuum pressure. This can be accomplished by applying load constraints during the theoretical wing design optimization process.

5.2 Avoiding Strong Spanwise Flow

To avoid strong spanwise flow it is necessary to prohibit the development of increasing negative pressures near the wing tip. Theoretical studies, such as shown in Figure 18, indicate that wing thickness pressures which build up near the wing tip are a major contributor to the tip pressures.

Fortunately, as shown in Figure 18, the wing outboard thickness pressures are relatively insensitive to changes in the airfoil shape or thickness on the inboard wing. To limit spanwise flow, the wing tip must be kept thin. However, the inboard portion of the wing can be thickened to satisfy structural requirements without affecting the spanwise flow. It is necessary, therefore, to consider the effect of wing thickness on drag-due-to-lift optimizations even in linearized flow calculations.

5.3 Avoiding Inboard Shock Separation

The formation of the forward shock as shown in Figure 19 is associated with flow conditions near the inboard portion of the wing and therefore is referred to as the inboard shock. This shock is associated with the flow near the wing leading-edge junction with the body[20,21]. The local flow on the upper surface of a swept wing is directed inward. The flow must then turn to run parallel to the local body surface. This subsequent turning of the flow causes compression waves; these may coalesce and form a shock wave that is swept aft at approximately the local flow Mach angle. If the required turning angle is large enough, the shock strength may become sufficiently strong to separate the boundary layer.

Empirical separation data[22,23,24] for flow across a glancing shock wave in which the flow is deflected in the place of the wing, indicate that a pressure rise of 50 percent across the shock will cause flow separation. Using simple sweep theory, the local flow turning angle (δ_M) can be related to the freestream Mach number, M_∞, wing leading-edge sweep, Λ, and local Mach number, M_ϱ (or pressure coefficient). If it is then assumed that the flow turns abruptly to flow parallel to the body surface, the oblique shock relations can be used to calculate the pressure rise associated with the abrupt change in direction. Flow separation across a forward shock is likely to occur[25] when this pressure rise exceeds 50 percent, as shown by the experimental data in Figure 19.

It is possible, therefore, to establish a limit on the allowable negative pressure coefficient level in the area of the wing/body junction. This limit, which depends on the wing sweep, local body curvature, and freestream Mach number, is usually significantly more restrictive than the aforementioned 80 percent vacuum limit.

The equations used to calculate the inboard shock limiting pressures are shown in Figure 19. Figure 20 shows the effect of freestream Mach number and leading-edge sweep on the inboard limiting pressure for a straight-sided body ($\delta_B = 0^O$). Body contouring, as shown in Figure 21, has a powerful effect on the allowable inboard pressures. A contracting body near the leading-edge junction typical of an area-ruled body greatly increases the allowable negative pressure, and also contributes a negative pressure field to the front portion of a wing. Hence the net benefit of body contouring in avoiding the formation of the inboard shock requires specific evaluations.

The same separation criterion (i.e., pressure rise of 50 percent) can be used to gauge the possibility of flow separation on the wing across glancing shocks produced by the body pressure field or other adjacent components such as nacelles, struts or tip fins. As shown in Figure 22, the local pressure field on the upper surface of a wing can amplify the pressure rise across a shock wave, causing a normally mild shock to promote separation. The fuselage, therefore, has an important effect on the design of supersonic wings.

5.4 Avoiding Trailing-Edge Separation Criteria

Wing planforms having a supersonic trailing edge develop a trailing-edge shock across which the wing upper surface pressures adjust to approximately freestream static pressure. The strength of the trailing-edge shock is directly associated with the upper surface pressure at the trailing edge, Figure 23. The flow across the trailing shock is quite similar to flow across a compression corner. Empirical correlations of separation data for compression corners[26,27] as shown in Figure 23 indicate that a pressure rise exceeding $1 + 0.3M_\ell^2$ can result in flow separation. Additional experimental studies[28,29] of flow across swept compression corners suggest that the effect of trailing-edge sweep can be accounted for by the use of the local normal Mach number $(M_{N\ell} = M_\ell \cos \Lambda_{TE})$ in determining the allowable pressure rise.

Relating the Mach number normal to the trailing edge to the freestream conditions gives the limiting edge pressures shown in Figure 24. Trailing-edge sweep is seen to have a powerful degrading effect on the allowable negative pressures near the trailing edge of a highly swept wing.

6.0 Separation Criteria Applications

This section contains applications of these design criteria to explain the flow development phenomena. The examples selected include the models used to illustrate the types of flow breakdown on the upper surface of supersonic wings in Section 4 (Figures 15 and 16).

The calculated separation criteria limiting upper surface pressures for a 75-degree swept-wing wind-tunnel model are shown in Figure 25. The inboard shock separation limiting pressure and the trailing-edge shock separation pressure are seen to be more restrictive than the 0.8 vacuum suction pressure limit. The local body slope (−5 degrees) in the area of the wing intersection nearly doubles the allowable pressure in the inboard regions of the wing. The application of the limiting pressure to this model as shown in Figure 26 predicted the development of the trailing-edge shock ($\alpha = 0^O, 2^O$) followed by formation of the inboard shock ($\alpha = 4^O$) and finally a large area of separated flow behind the merged inboard and trailing edge shocks ($\alpha = 6^O$). Prediction of the inboard movement of the trailing-edge shock separation as angle of incidence increases is shown in Figure 27.

The design criteria have been used to explain the development of the shock-induced separation on the model shown in Figure 16 when the conical mid-body section was replaced by a curved mid-body[30]. The calculated theoretical pressures[31] shown in figure 28 indicate that the curved mid-body produced a strong mid-body shock that far exceeded the limiting pressure rise ($P2/_{P1} = 1.5$) across a glancing shock wave.

The flow development on another wind-tunnel model designed to achieve a uniform load distribution at Mach 3.0 is shown in Figure 29 at approximately the design lift coefficient ($C_L = 0.10$). Application of the design criteria to this model indicates that separation behind strong inboard and trailing-edge shock waves is very likely. The flow visualization picture and pressure contour plot confirmed these predictions. Figure 30 illustrates how the nonlinear pitching moment characteristics of this model can be interpreted by means of the flow separation criteria. The initial break in the pitching moment curve is associated with loss of lift near the wing tip caused by trailing edge separation. Severe pitch-up results as the separation behind the inboard shock rolls up into a spiral vortex sheet, shifting the wing lift inboard and forward.

The separation criteria have been applied to the 70-degree, cambered, swept-wing design for which the drag and lift data were shown in Figure 12. As shown in Figure 31, the separation criteria indicate that a trailing-edge shock would develop above the design lift coefficient ($C_L = 0.08$) followed at higher incidences by development of leading-edge vortex separation and possible tip separation associated with theoretically high suction pressures near the tip.

The envelope drag-due-to-lift factors ($KE = (\alpha C_D/\alpha C_L^2)_{min}$) for a series of flat and twisted wings are shown in Figure 32. All of these wings had the same planform geometry but different airfoils. The 2.5-percent, thick, cambered, twisted wing achieved approximately 20 percent lower drag due to lift than any of the other wing designs tested. Interpretation of the theoretical pressure distributions by means of the separation criteria would indicate that the higher drag-due-to-lift levels on the various wing designs were associated with different flow mechanisms. The thin, sharp-edge, flat-wing flow was dominated by leading-edge separation. The increased thickness

on the flat wing appears to have suppressed the development of the leading-edge vortex. However, the separation criteria would indicate flow breakdown because of a strong trailing-edge shock and high suction pressure near the wing tip. The thicker cambered wing experienced strong spanwise flow and severe trailing-edge shock separation.

The example applications of the separation criteria in this section are passive applications, used to explain the flow breakdown on unsuccessful wing designs that were tested before the design criteria were developed. These applications illustrate the validity of these simple design criteria. The design applications shown in the next section illustrate successful wing designs developed to satisfy the design criteria.

7.0 Design Applications of the Separation Criteria

The wing development method using the supersonic wing design criteria is summarized in Figure 33. The wing/body combination is designed using linear theory to achieve low theoretical drag while satisfying the wing structural depth and volume requirements. The theoretical wing upper surface pressure distribution is calculated at the design condition accounting for wing thickness, camber, twist, and body effects. The theoretical pressure distribution is checked to determine if any of the design criteria have been violated. If the design criteria are satisfied, the wing design is considered to have a high probability of success, if they are not, the design must be modified.

Figure 34 illustrates the development of a tailored wing design to provide additional wing inload thickness. Theory indicates that the only drag difference between the two wing designs would be that due to thickness wave drag, independent of lift coefficient. Tests conformed these designs.

The wind-tunnel results shown in Figure 35 verified the low drag due to lift of an early U.S. SST wing. The achieved level of drag due to lift was near to the theoretical optimum drag level. This is considerably better than would be achieved with an uncambered wing.

A relatively unexplored application of the design criteria is shown schematically in Figure 36 by the typical theoretical flow breakdown boundaries. The example illustrates a design condition free of predicted flow separation. At the indicated off-design maneuvering condition, the wing design would encounter flow breakdown. This suggests the possibility of using variable camber to expand the separation-free operating conditions. The supersonic wing design criteria could be quite useful in such an application.

8.0 Conclusions

The foregoing discussions have shown that highly swept wings offer low supersonic drag levels.

Highly swept flat wings are unable to achieve the theoretically low-drag-due-to-lift levels except at very small incidence angles.

Highly swept cambered and twisted wings designed for optimum load distributions with finite body-edge pressures can achieve low drag levels providing the flow remains attached at the design condition.

Supersonic design criteria have been presented as a means of avoiding shock-induced flow separations and thereby allowing the attached flow condition to be achieved. The supersonic wing design methods of Ref. 31 allow the design constraints to be imposed during the wing design process.

Acknowledgements

References

1. Brown, C. E., and McLean, F. E., "The Problem of Obtaining High Lift Drag Ratios at Supersonic Speeds." *J.A.S.* May, 1959, pp 298-302.

2. *Proceedings of the SCAR Conference.* NASA CP-001, Vol. I and Vol. II, November 1976; USAF AFFDL, Feb. 1976.

3. *Design Conference Proceedings: Technology for Supersonic Cruise Military Aircraft.* Vol. I and Vol. II.

4. Carlson, H. W., *Aerodynamic Characteristics at Mach Number 2.05 of a Series of Highly Swept Arrow Wings Employing Various Degrees of Twist and Camber.* NASA TMX-332, June 1960.

5. Carlson, H. W., *Longitudinal Aerodynamic Characteristics at Mach Number 2.02 of a Series of Wing-Body Configurations Employing a Cambered and Twisted Arrow Wing.* NASA TMX-838, May 1963.

6. Ornberg, T., *A Note on the Flow Around Delta Wings.* KTH-Aero TN38, Feb. 1954.

7. Kuchemann, D., "Types of Flow on Swept Wings." *Journal of the Royal Aeronautical Society,* Vol. 57, pp 683-699, Nov. 1953.

8. Stanbrook, A., and Squire, L. C., "Possible Types of Flow at Swept Leading Edges." *The Aeronautical Quarterly,* Feb. 1964, pp 72-82.

9. Ghorai, S. C., "Leading-Edge Vortices and Shock-Detachment Flow Over Delta Wings." *Journal of Aircraft,* Vol. 6, No. 3; May-June 1969, pp 228-232.

10. Polhamus, E. C., *A Concept on the Vortex Lift of Sharp-Edge Delta Wings Based on a Leading-Edge-Suction Analogy of Vortex Lift to the Drag Due to Lift of Sharp-Edge Delta Wings.* NASA TN D-4739, May 1968.

11. Polhamus, E. C., "Predictions of Vortex-Lift Characteristics by a Leading-Edge Suction Analogy." *Journal of Aircraft,* Vol. 8, No. 4, April 1971.

12. Snyder, M. H. Jr., and Lamar, J. E., *Application of the Leading-Edge-Suction Analogy to Prediction of Longitudinal Load Distribution and Pitching Moment for Sharp-Edge Delta Wings.* NASA TN D-6994, Sept. 1972.

13. Carlson, H. W., *Pressure Distribution at Mach Number 2.05 on a Series of Highly Swept Arrow Wings Employing Various Degrees of Twist and Camber.* NASA TN D-1264, March 1962.

14. Squire, L. C., Jones, J. G., and Stanbrook, A. "An Experimental Investigation of the Characteristics of Some Plane and Cambered 65° Delta Wings at Mach Numbers from 0.7 to 2.0." R.A.E., Rept. and Memo No. 3305, July 1961.

15. Squire, L. C., "The Estimation of the Delta Wing Lift of Delta Wings at Supersonic Speeds." *Journal of the Royal Aeronautical Society,* Vol. 67, Aug. 1963.

16. Fellows, K. A., and Carter, E. C., *Results and Analysis on Two Isolated Slender Wings and Slender Wing-Body Combinations at Supersonic Speeds, Part I, Analyses.* ARC C.P. 1131, 1970.

17. Manro, M. E., Bobbit, P. J., and Rogers, J. T., *Comparisons of Theoretical and Experimental Pressure Distributions on an Arrow-Wing Configuration at Subsonic, Transonic, and Supersonic Speeds.* Paper No. 11, AGARD CP-204, Sept. 1976.

18. Smith, A. M. O., "High Lift Aerodynamics." *Journal of Aircraft,* Vol. 12, No. 5, June 1975.

19. Sigalla, A., *Design Criterion on Upper Surface Inboard Pressure Coefficient for Arrow Wings.* Boeing Document D6-4142TN, Oct. 1962.

20. Rogers, E. W. E., and Hall, I. M., "An Introduction to the Flow About Plane Swept-back Wings at Transonic Speeds." *Journal of the Royal Aeronautical Society*, Vol. 64, No. 596, Aug. 1960.

21. Stanbrook, A., *An Experimental Study of the Glancing Interaction Between a Shock Wave and a Turbulent Boundary Layer.* ARC CP No. 555, 1960.

22. McCabe, A., "The Three Dimensional Interaction of a Shock Wave With a Turbulent Boundary Layer." *The Aeronautical Quarterly*, Aug. 1966.

23. Lowrie, B. W., *Cross-Flows Produced by the Interaction of a Swept Shock Wave with a Turbulent Boundary Layer.* PhD Thesis, University of Cambridge, Dec. 1965.

24. Korkegi, R. H., " A Simple Correlation for Incipient Turbulent Boundary-Layer Separation Due to a Skewed Shock Wave." *AIAA Journal,* Vol. 11, No. 11, Nov. 1973, pp 1578-1579.

25. Korkegi, R. H., "Comparison of Shock-Induced Two- and Three-Dimensional Incipient Turbulent Separation," *AIAA Journal,* Vol. 13, No. 4, April 1975, pp 534-535.

26. Kuehn, D. M., "Experimental Investigation of the Pressure Rise Required for the Incipient Separation of Turbulent Boundary Layers in Two-Dimensional Supersonic Flow." NASA Memo 1-21-59A, Feb. 1959.

27. Stalker, R. J., "Sweepback Effects in Turbulent Boundary-Layer Shock-Wave Interaction." *J.A.S.,* May 1960.

28. Green, J. E., *Interactions Between Shock Waves and Turbulent Boundary Layers."* R.A.E. Tech. Report 69069, May 1969.

29. Kulfan, R. M., *Prediction of Body Induced Boundary Layer Separation on a Swept Wing."* Boeing Document D6A-10961-1TN, April 1967.

30. Middleton, W. D., and Lundry, J. L., *A Computational System for Aerodynamic Design and Analysis of Supersonic Aircraft.* NASA CR-2715, March 1976.
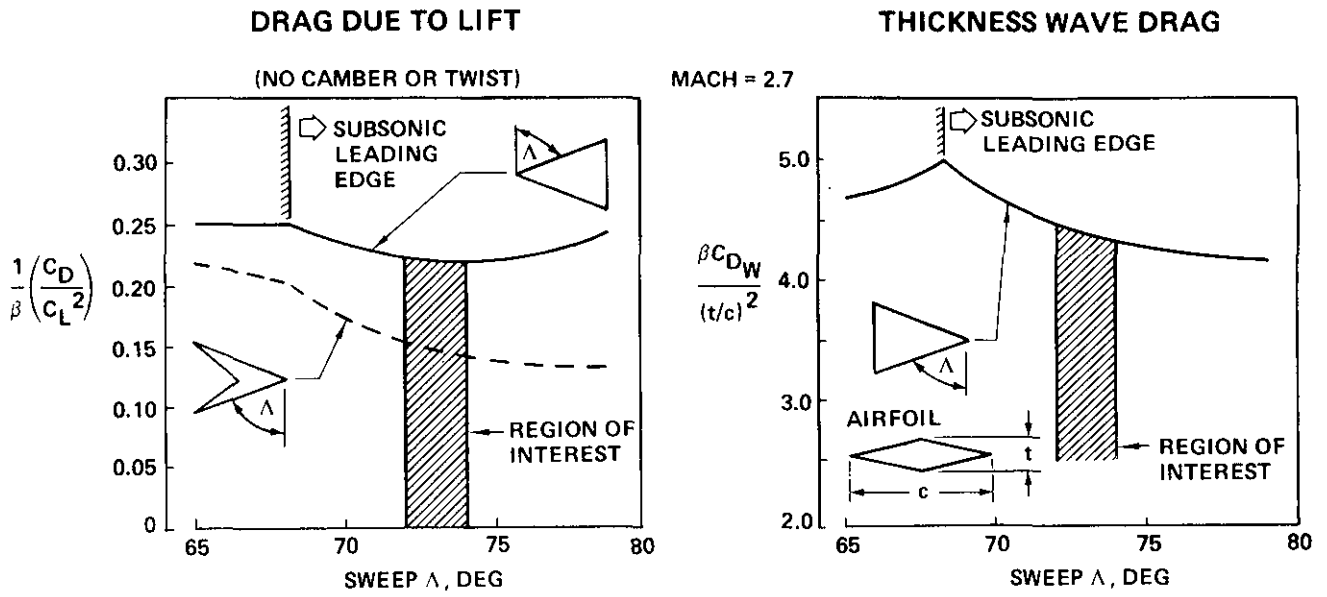
DRAG DUE TO LIFT

(NO CAMBER OR TWIST)

MACH = 2.7

THICKNESS WAVE DRAG

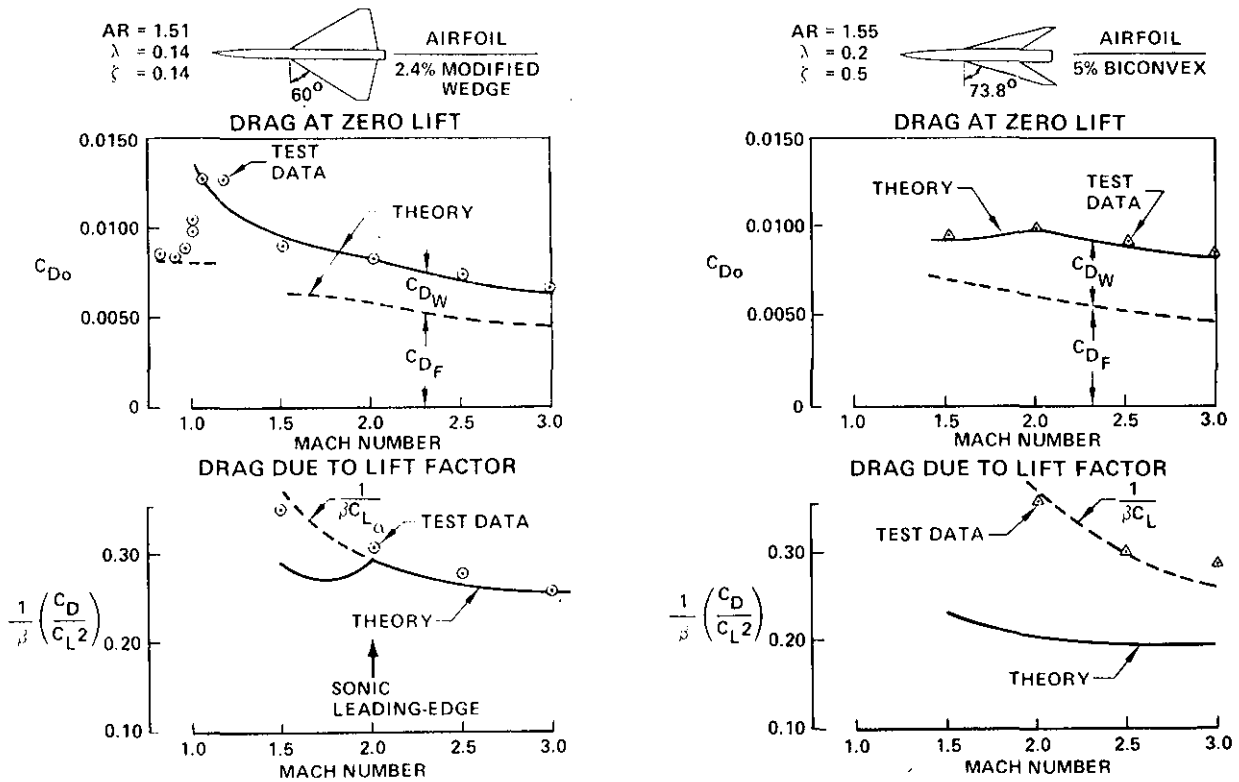Figure 1   Supersonic Wing Planforms

Figure 2   Comparison of Theory with Experiment for Symmetric Supersonic Wings

9

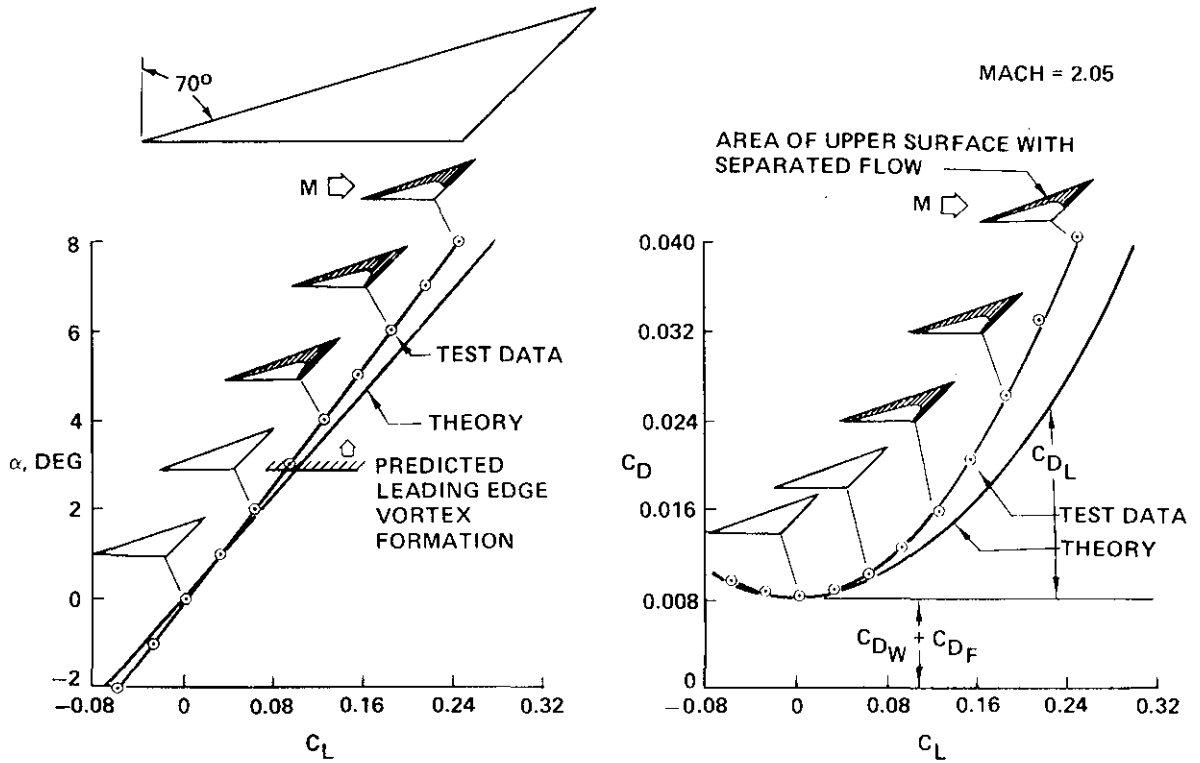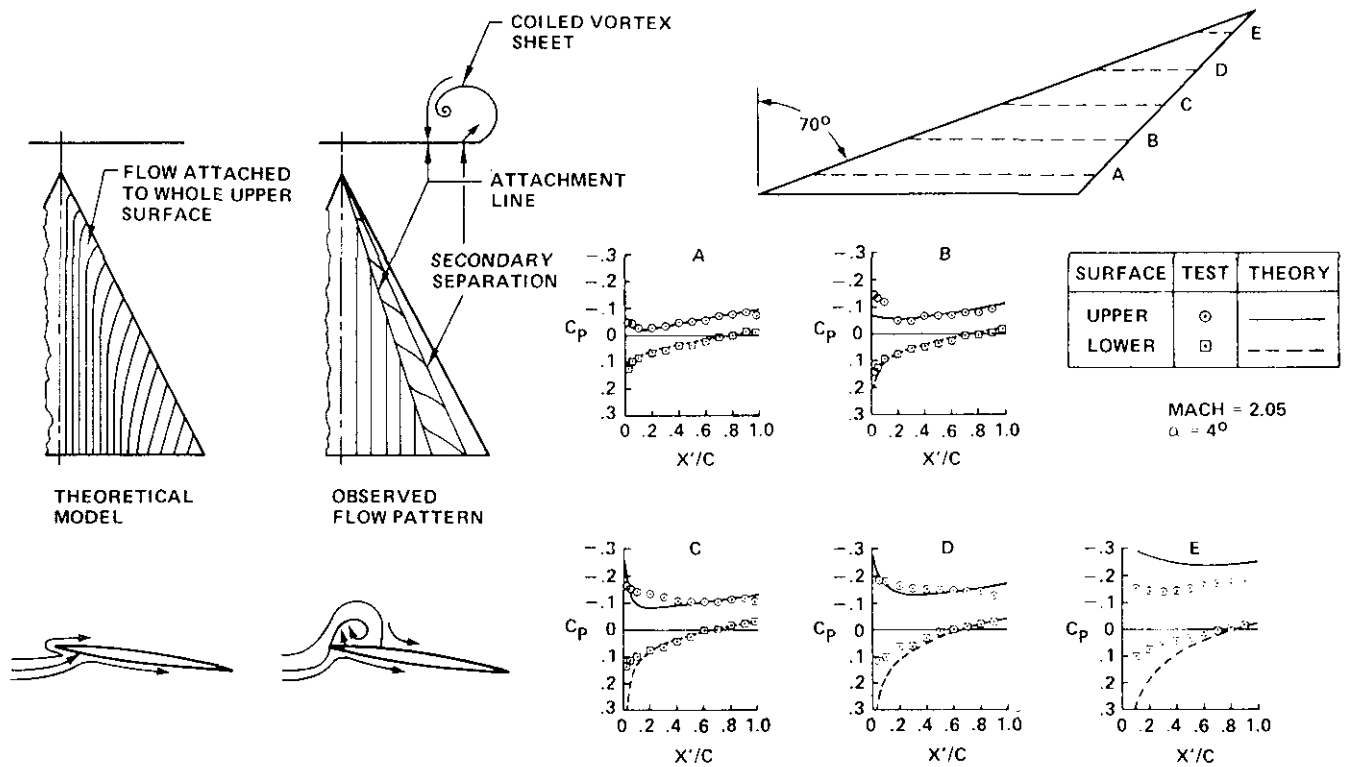Figure 3   Lift and Drag of a Highly Swept Flat Wing

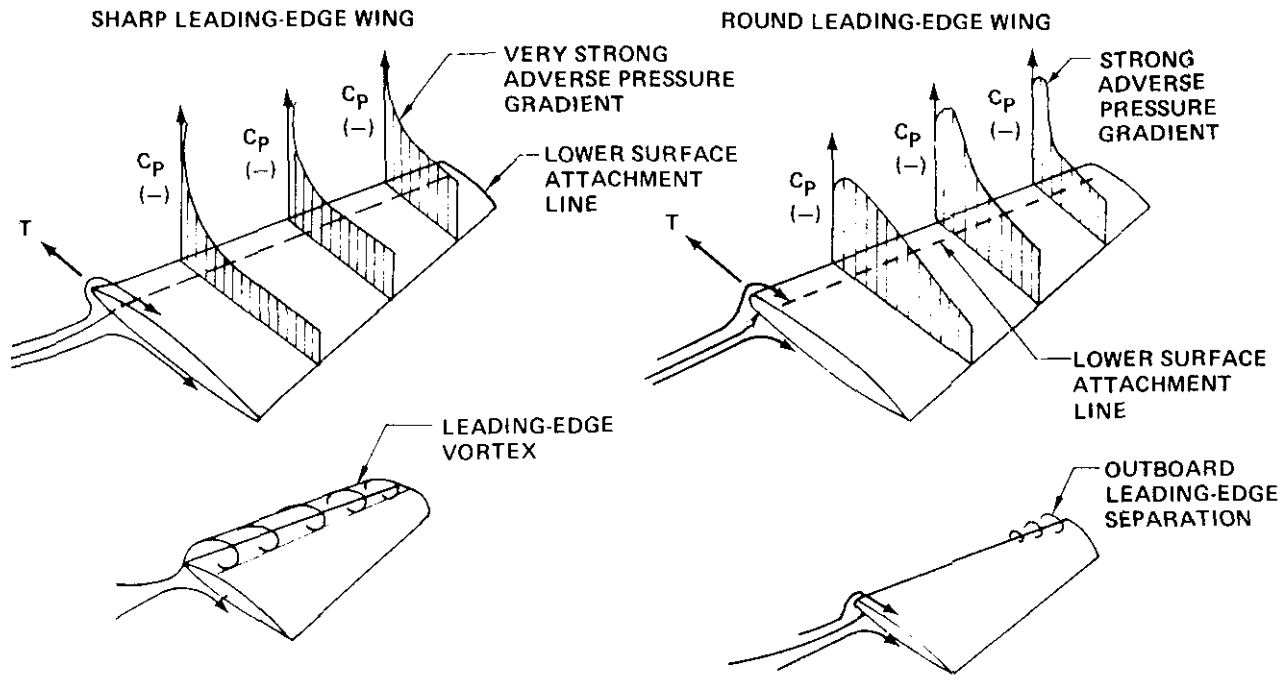Figure 4   The Practical Problem of the Highly Swept Wing

10

SHARP LEADING-EDGE WING

C_P (−)

C_P (−)

C_P (−)

T

--- VERY STRONG ADVERSE PRESSURE GRADIENT

—LOWER SURFACE ATTACHMENT LINE

LEADING-EDGE VORTEX

ROUND LEADING-EDGE WING

C_P (−)

C_P (−)

C_P (−)

T

— STRONG ADVERSE PRESSURE GRADIENT

—LOWER SURFACE ATTACHMENT LINE

—OUTBOARD LEADING-EDGE SEPARATION

Figure 5   Pressure Distributions on Highly Swept Flat Wings

65°

A —·—·—·— A

SYMBOL	AIRFOIL	CAMBER	LEADING EDGE
⊙	BICONVEX	NONE	SHARP
△	RAE 101		ROUND
⊡		CONICAL	

C_T $C_L \alpha$

M →

α

$C_{D_F} + C_{D_W}$

SYMMETRIC WINGS

$C_T + (C_{D_W} + C_{D_F}) = C_D - \alpha C_L$

MACH = 1.62

CONICAL CAMBERED WING

$C_T + (C_{D_W} + C_{D_F}) = C_D - \alpha (C_L - C_{L_M})$

$C_{D_W} + C_{D_F}$

— LOSS OF LEADING-EDGE SUCTION

— SHARP LEADING EDGE

TEST DATA

— ROUND LEADING EDGE

— THEORY —

RAE 101 AIRFOIL

— PLANE WING

STATION A-A

— CAMBERED WING

0.0200

0.0150

0.0100

0.0050

−0.20   −0.10   0   0.10   0.20

C_L

0.0200

0.0150

0.0100

0.0050

$C_{D_F} + C_{D_W}$

TEST DATA

C_{L_M}

−0.20   −0.10   0   0.10   0.20

C_L

Figure 6   Effect of Airfoil Geometry on Chord Force

$\alpha_N = TAN^{-1} (TAN \alpha/COS \Lambda)$

MACH = 2.05
Λ = 70°

$M_N = M COS \Lambda \sqrt{1 + SIN^2 \alpha TAN^2 \Lambda}$

SHARP LEADING-EDGE AIRFOILS

$\alpha_N = TAN^{-1} (TAN \alpha/COS \Lambda)$

LEADING EDGE SEPARATION

NASA DATA
M = 2.05

$M_N = 0.6 + 0.013 \alpha_N$

70°

ATTACHED FLOW

$M_N = M COS \Lambda \sqrt{1 + SIN^2 \alpha TAN^2 \Lambda}$

ROUND LEADING-EDGE AIRFOILS

$\alpha_N = TAN^{-1} (TAN \alpha/COS \Lambda)$

LEADING-EDGE SEPARATION

ATTACHED FLOW

$M_N = M COS \Lambda \sqrt{1 + SIN^2 \alpha TAN^2 \Lambda}$
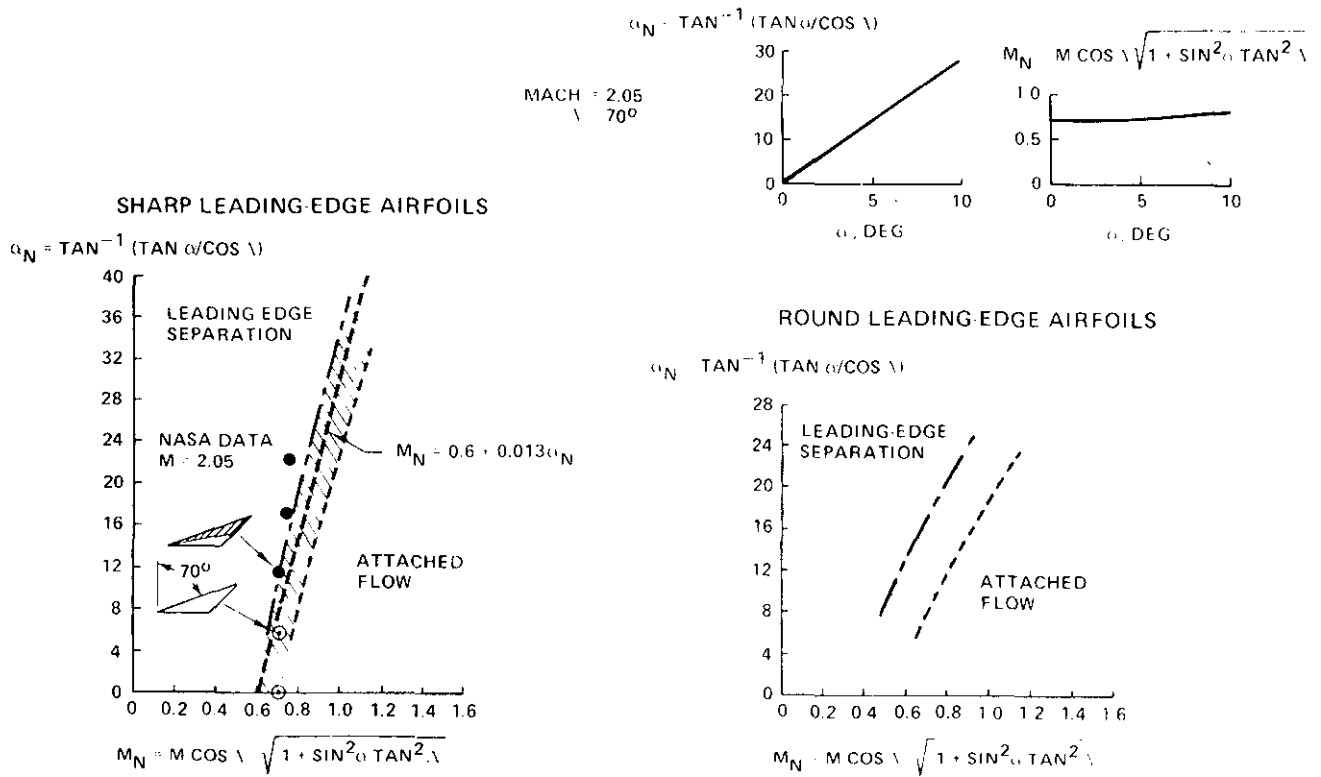
Figure 7   Flat Wing Leading-Edge Separation Boundaries

$\Lambda_{LE} = 50°$

$\Lambda_{LE} = 60°$

$\Lambda_{LE} = 70°$

$\Lambda_{LE} = 75°$

ANGLE OF ATTACK, α

ORDERED LEADING EDGE VORTEX FLOW

ATTACHED FLOW

MACH NUMBER
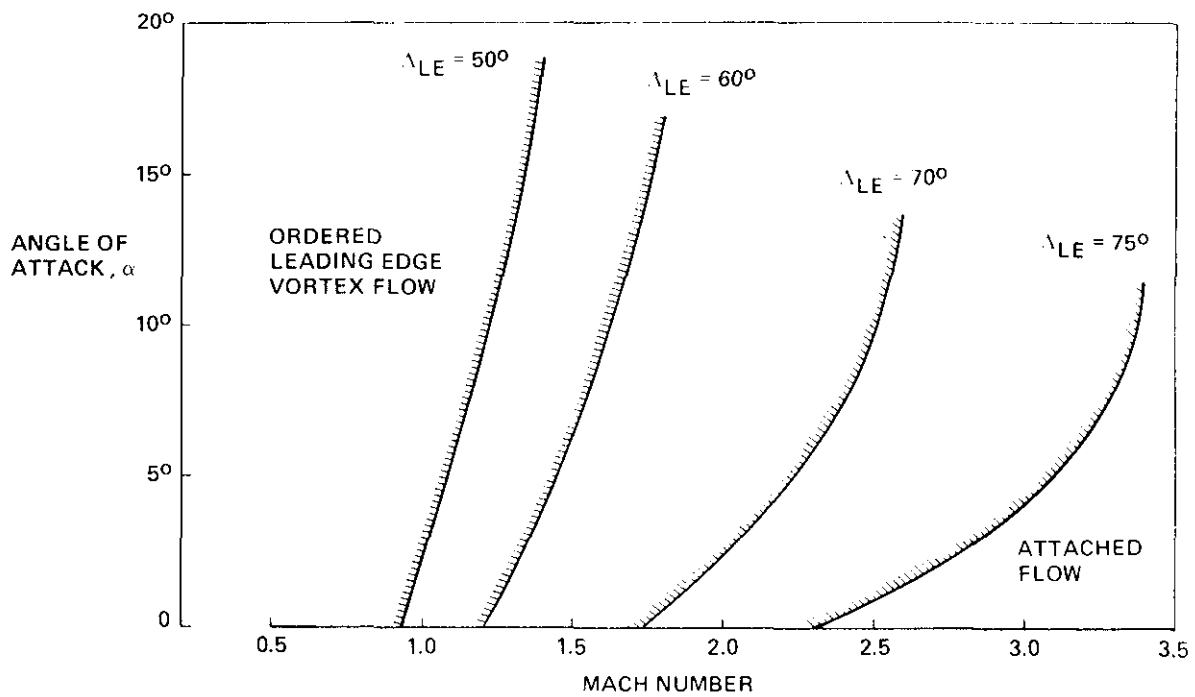
Figure 8   Ordered Leading-Edge Vortex Formation Boundaries for Flat Sharp Swept Wings

- **LEADING-EDGE SWEEP**
- **LEADING-EDGE RADIUS**
- **CAMBER – DROOP**
- **TWIST**

DISPLACEMENT OF LEADING-EDGE SEPARATION WITH CAMBER

APEX

MACH = 2.0

TRAILING EDGE

A = 0.75

α_N

LEADING-EDGE SEPARATION

ATTACHED FLOW

M_N

α_N

ATTACHED FLOW

M_N

LEADING-EDGE SEPARATION

APEX

ATTACHED FLOW

SHARP EDGE AIRFOIL BOUNDARIES

EXPERIMENTAL OBSERVATIONS

SEPARATED FLOW

TRAILING EDGE

α, DEG

0   2   4   6   8   10

LEADING-EDGE VORTEX SEPARATION ON A GOTHIC WING

Figure 9   Factors Affecting Leading-Edge Vortex Formation Boundary

AT DESIGN INCIDENCE

C_P (−)

T

ABOVE DESIGN INCIDENCE

ADVERSE PRESSURE GRADIENT

C_P (−)

LOWER SURFACE ATTACHMENT LINE

BELOW DESIGN INCIDENCE

ADVERSE LOWER SURFACE PRESSURE GRADIENT

UPPER SURFACE ATTACHMENT

C_P (−)
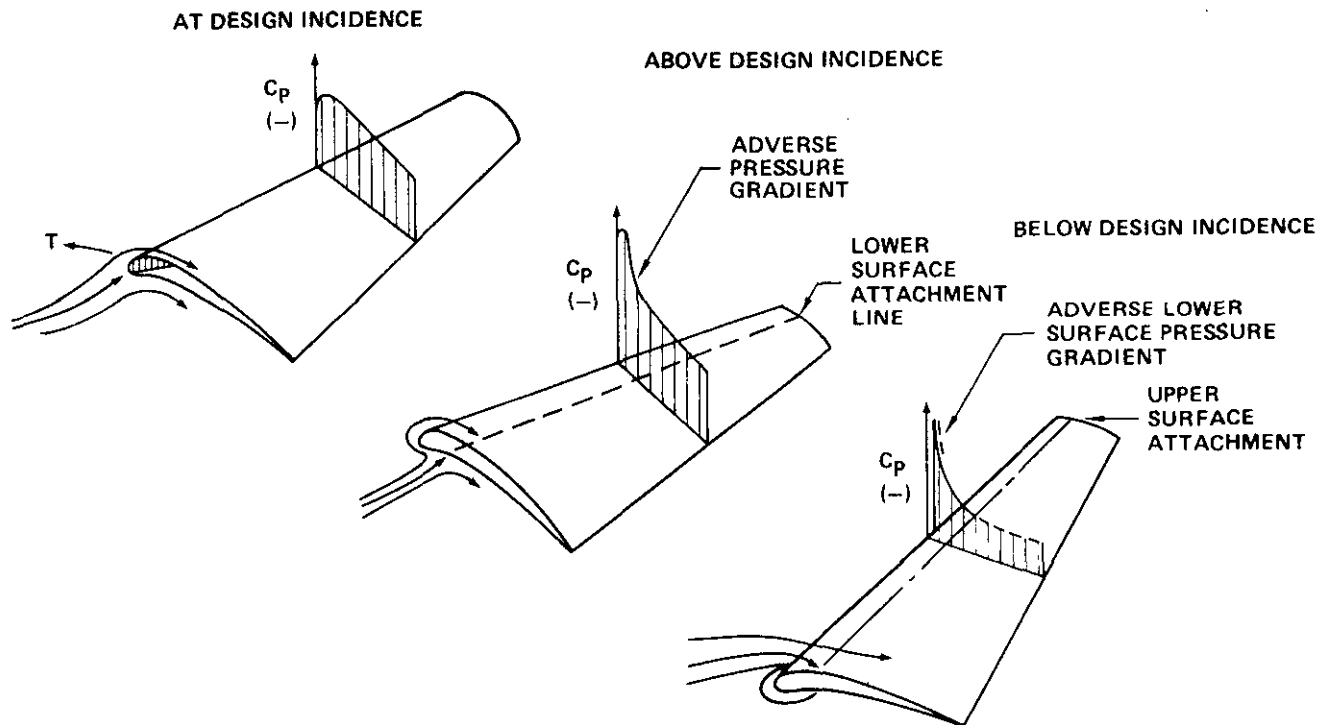
Figure 10   Pressure Distribution on Highly Swept Cambered Wings

13
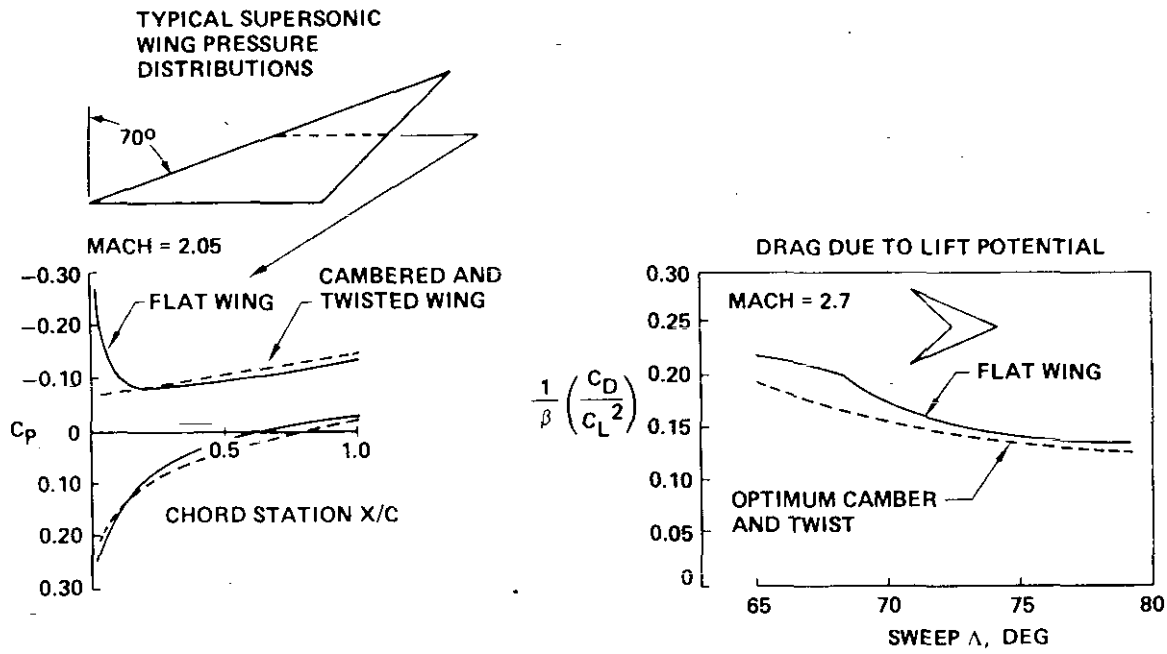
Figure 11   Effect of Wing Camber and Twist on Theoretical Results
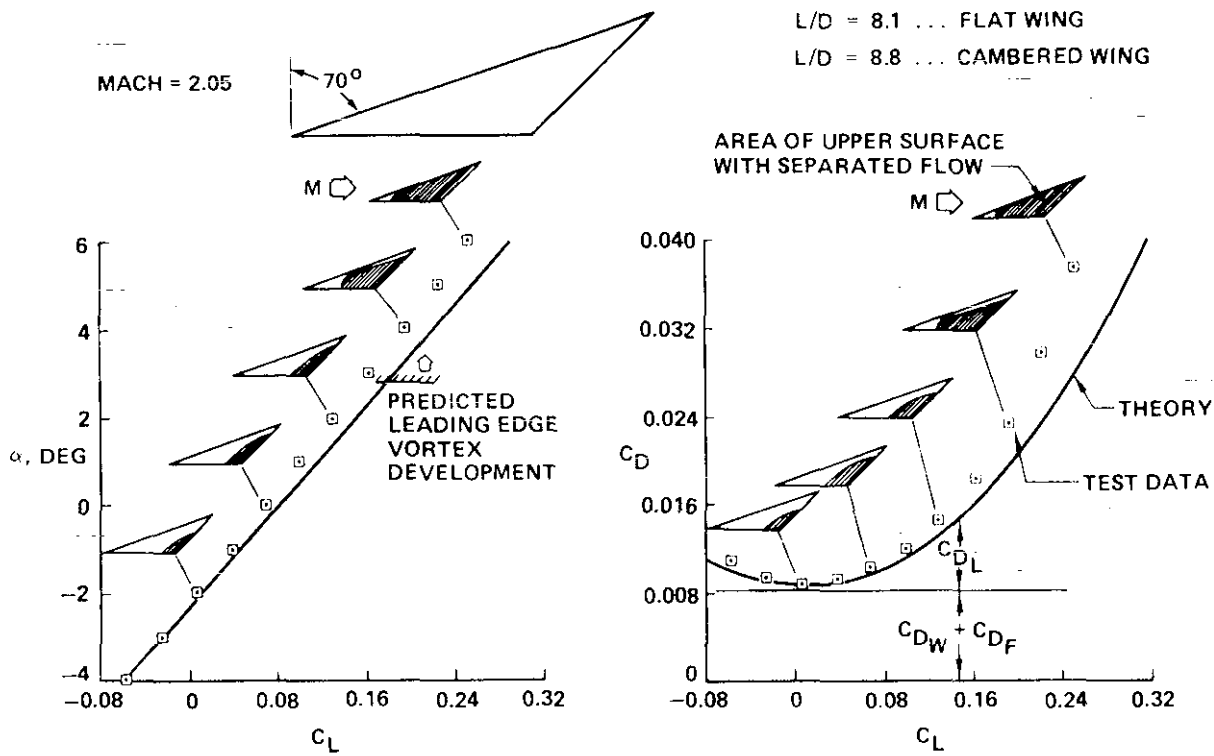
Figure 12   Lift and Drag of a Highly Swept Cambered and Twisted Wing

14

LIFT/DRAG RATIO

WING W1
DESIGN POINT M = 2.5; C_L = 0.10

10

9

8

$(L/D)_{MAX}$

7

6

5

25%

16.5%

WING W2
DESIGN POINT
M = 2.0; C_L = 0.13

FLAT
WING

ALL WINGS HAVE
SAME PLANFORM

BOEING SUPERSONIC WIND
TUNNEL DATA

1.0   1.5   2.0   2.5   3.0   3.5
MACH NUMBER

PLANFORM

Λ_{LE} = 73.8°

$(t/c)_{MAX}$ = 2.5%

BALANCE
FAIRING

A   A

SECTION A-A
2.5% BICONVEX
AIRFOIL

C_L 0.14

0.18

$C_{D_{SYM}}$

CAMBERED
WING

UNCAMBERED
WING

C_D

$(C_D - C_{D_{SYM}}) = K_E C_L^2$

FLAT WING ZERO LIFT DRAG

.010

.00

$C_{D_{SYM}}$

.006

.004

.002

0

x

x

x

UNCAMBERED WING
TEST DATA

TRIP STRIP
DRAG

ESTIMATED
TURBULENT
SKIN FRICTION

THEORETICAL WING WAVE DRAG

THEORETICAL WAVE
DRAG OF WING AND
BALANCE FAIRING

1.0   1.5   2.0   2.5   3.0
MACH NO.

TRAILING EDGE | LEADING EDGE SUBSONIC | LEADING EDGE
SUBSONIC | TRAILING EDGE | SUPERSONIC
SUPERSONIC

ENVELOPE DRAG DUE TO LIFT FACTOR

0.6

0.5

0.4

K_E 0.3

0.2

0.1

0

WING
W_2

FLAT WING

THEORY OPTIMUM
CAMBER

WING
W_1

1.0   1.5   2.0   2.5   3.0   3.5
MACH NUMBER

Figure 13   The Effect of Camber and Twist on the Lift Drag Ratio of Highly Swept Wings

COILED VORTEX
SHEET

WEAK OBLIQUE
SHOCK WAVE

COILED
VORTEX
SHEET

OBLIQUE
SHOCK
WAVE

FLOW ATTACHED
TO WHOLE UPPER
SURFACE

ATTACHMENT
LINE

SECONDARY
SEPARATION

FLOW ATTACHED
TO WHOLE
UPPER SURFACE

FLOW DEFLECTED
THROUGH
SHOCK WAVE

SEPARATION
AT BASE OF
SHOCK WAVE

FLOW ATTACHED
TO SURFACE
NEAR LEADING
EDGE

ATTACHED FLOW

**LEADING-EDGE
VORTEX**

**ATTACHED FLOW
WITH WEAK
OBLIQUE SHOCK**

**FLOW SEPARATION
BEYOND STRONG
OBLIQUE SHOCK**

**ATTACHED FLOW
TO TRAILING EDGE**

**ATTACHED FLOW WITH STRONG
SPANWISE FLOW**

**SEPARATED FLOW BEHIND STRONG
TRAILING-EDGE SHOCK**

Figure 14   Main Types of Flow on Highly Swept Wings

MACH = 3.0

$\alpha = 0^0$
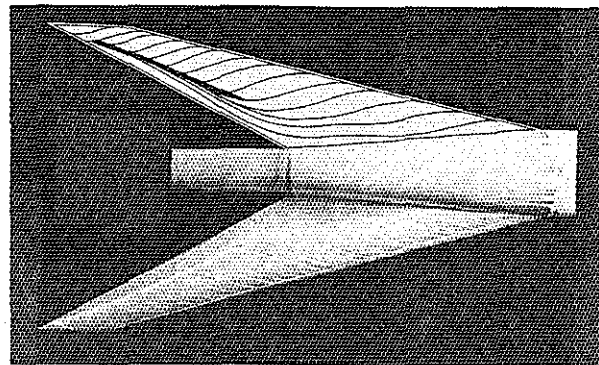
ATTACHED FLOW WITH STRONG
SPANWISE FLOW NEAR THE
TRAILING EDGE.

$\alpha = 2^0$
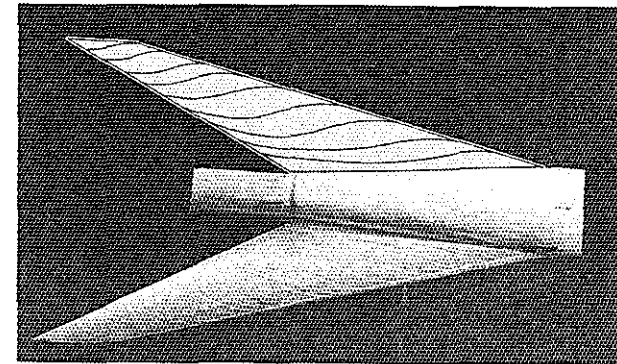
SEPARATION BEHIND STRONG
SHOCK NEAR THE TRAILING EDGE.

$\alpha = 4^0$
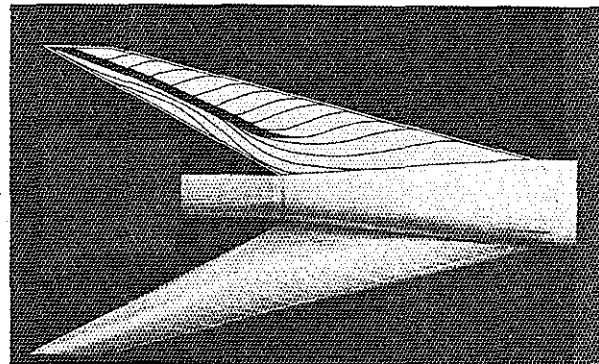
INCREASED SEPARATION BEHIND SHOCK
NEAR THE TRAILING EDGE, ADDITIONAL
SHOCK FORMING INBOARD.

$\alpha = 6^0$
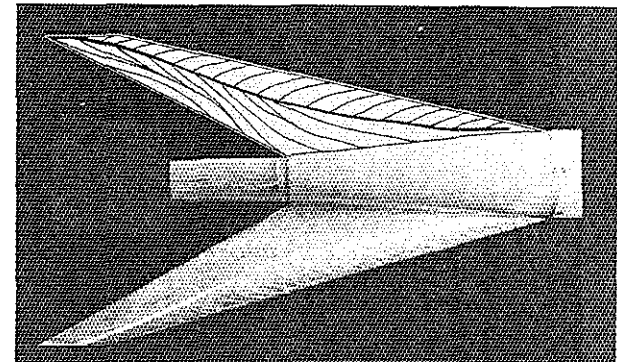
SEPARATION OVER MOST OF THE WING
BEHIND THE MERGED INBOARD
AND TRAILING EDGE SHOCKS.

Figure 15   Example of Shock Induced Separation
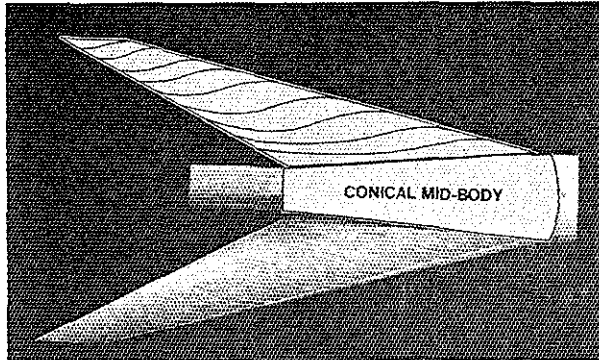
ATTACHED FLOW WITH STRONG
SPANWISE FLOW NEAR THE
TRAILING EDGE
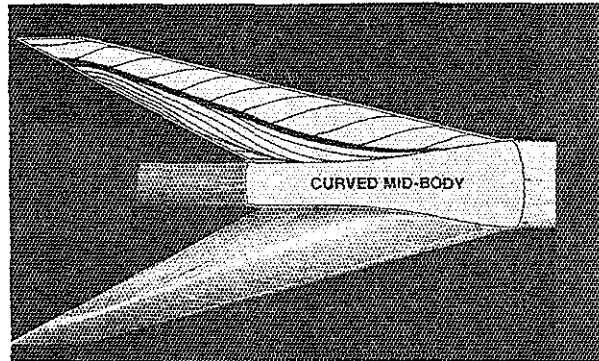
SEPARATED FLOW BEHIND
STRONG BODY INDUCED SHOCK
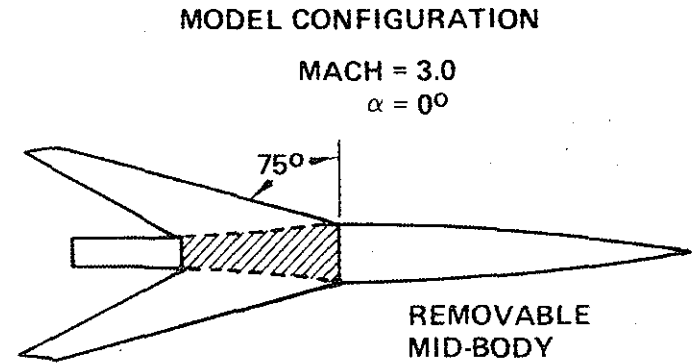
MODEL CONFIGURATION

MACH = 3.0
$\alpha = 0^{\circ}$

75°

REMOVABLE
MID-BODY

BODY CROSS-SECTIONAL
AREA DISTRIBUTION

CROSS SECTIONAL
AREA (INCHES^2)

CONICAL
MID-BODY

CURVED
MID-BODY

DISTANCE ALONG BODY (INCHES)
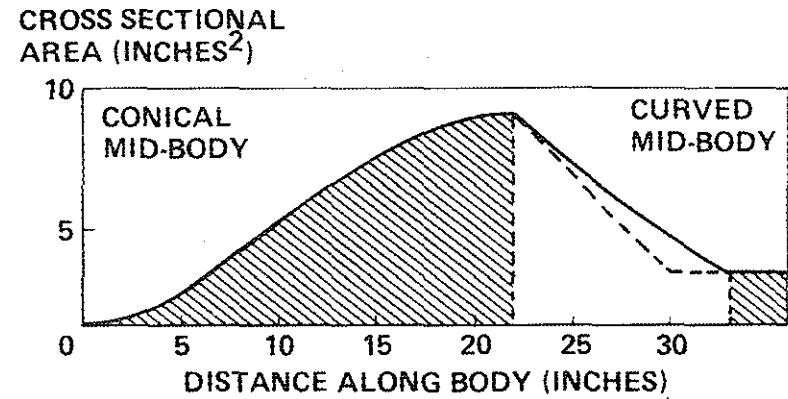
Figure 16   Body Induced Shock Separation
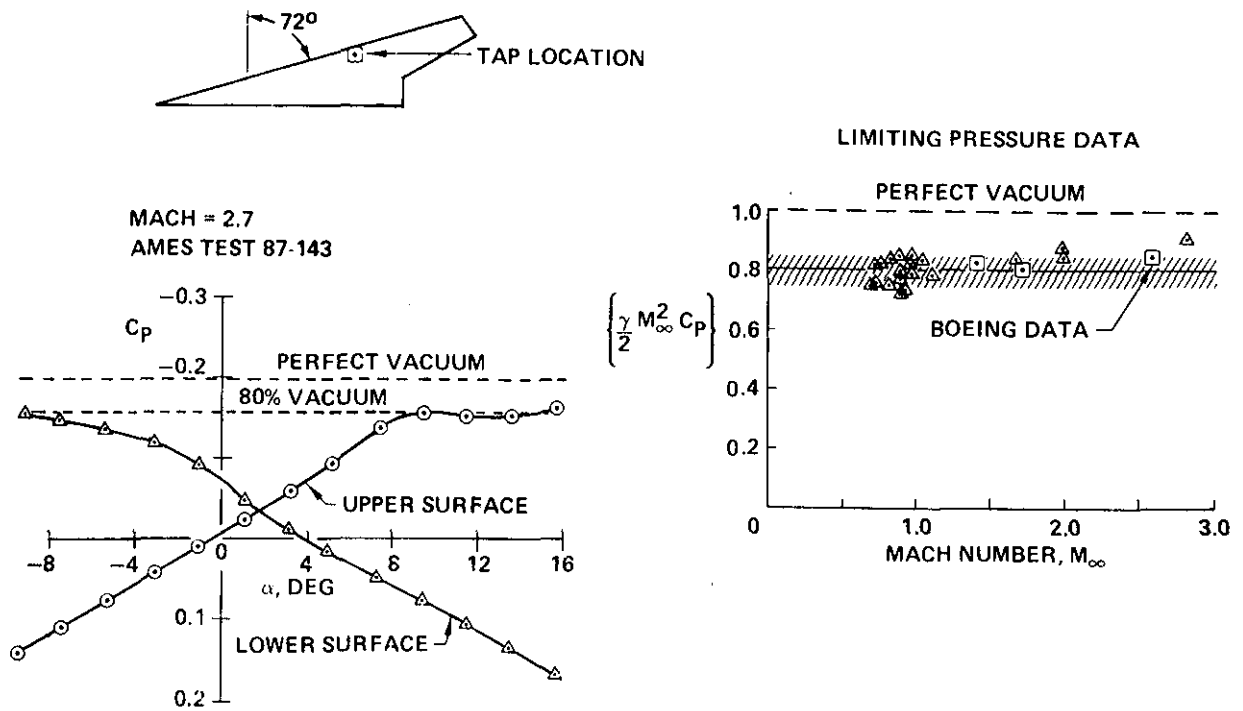
Figure 17   Limiting High Suction Pressures
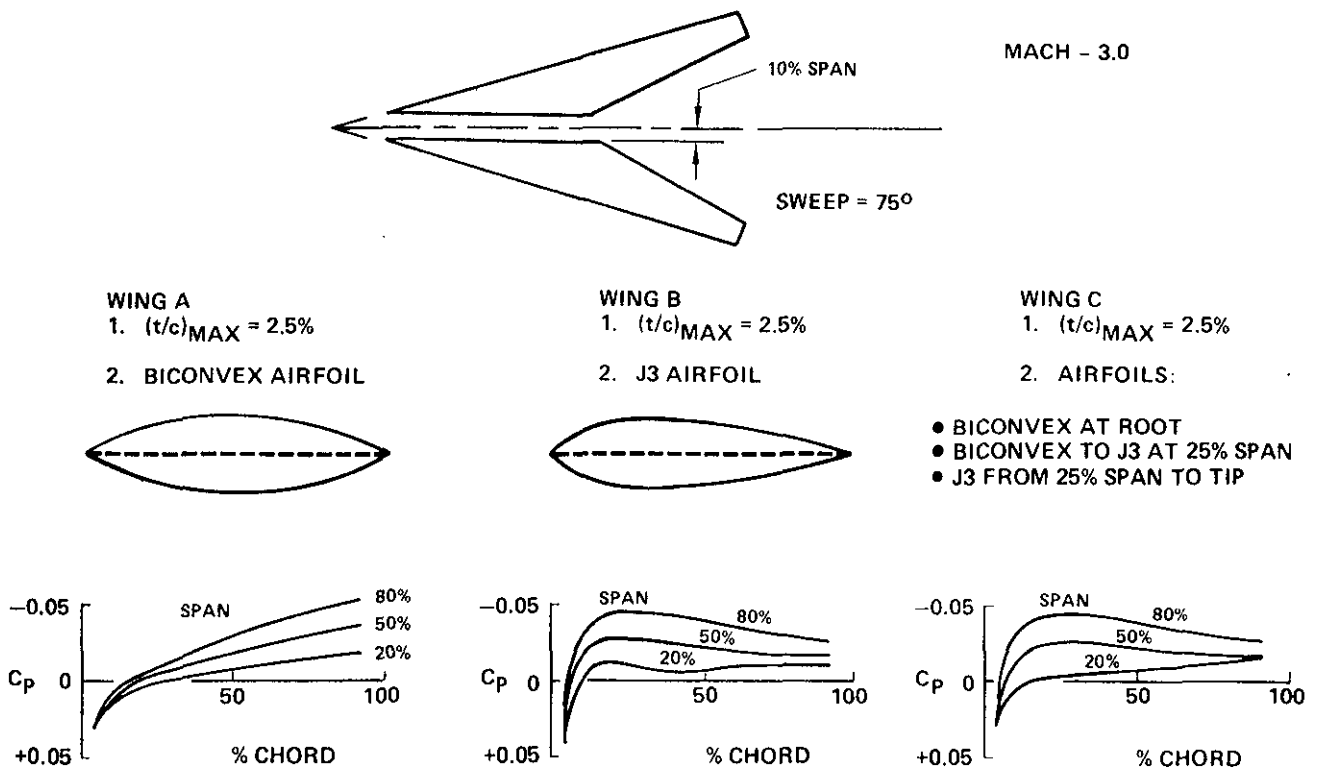
Figure 18   Limit Tip Thickness to Subdue Strong Spanwise Flow

$$\delta_T = \delta_M + \delta_B$$

$$\delta_M = \Lambda - \text{SIN}^{-1}\left\{ \text{SIN } \Lambda \left(\frac{M_\infty}{M_\ell}\right)\left[\frac{5 + M_\ell^2}{5 + M_\infty^2}\right]^{1/2}\right\}$$

OBLIQUE SHOCK RELATIONS:

$$\Theta = \text{SIN}^{-1}\sqrt{\frac{6\left(\dfrac{P_2}{P_1}\right)+1}{7M_\ell^2}}$$

$$\delta_S = \text{TAN}^{-1}\left\{\frac{1}{\text{TAN } \Theta\left[\dfrac{6M_\ell^2}{5(M_\ell^2 \text{ SIN}^2 (\Theta-1)} - 1\right]}\right\}$$

GLANCING SHOCK WAVE SEPARATION CRITERIA
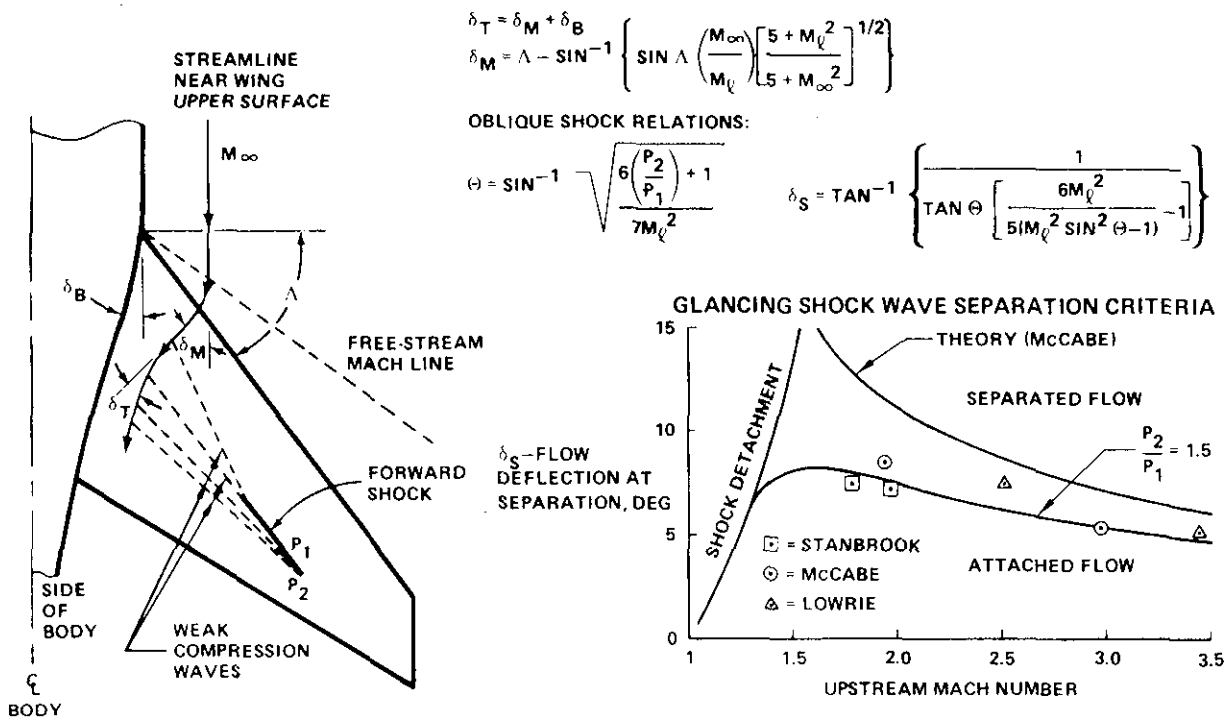
Figure 19   Inboard Shock Separation Criteria
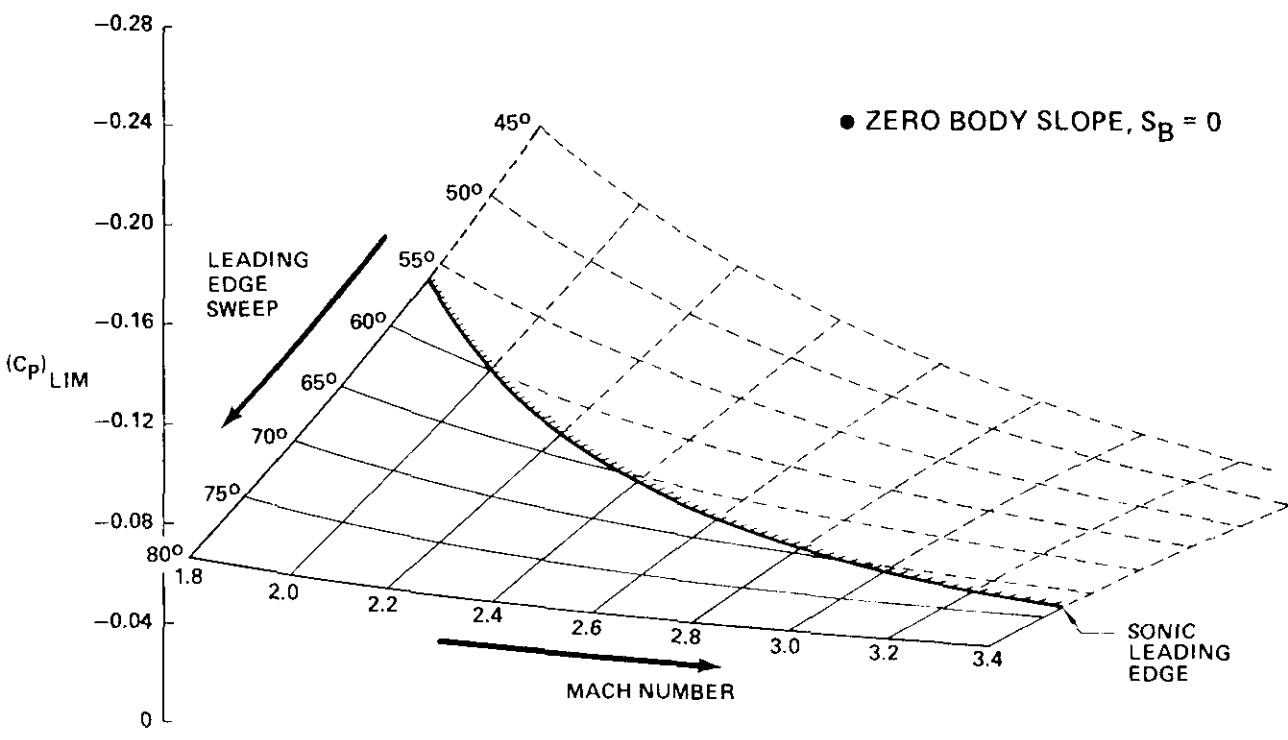
Figure 20   Effect of Sweep and Mach Number on Inboard Shock Criteria

20
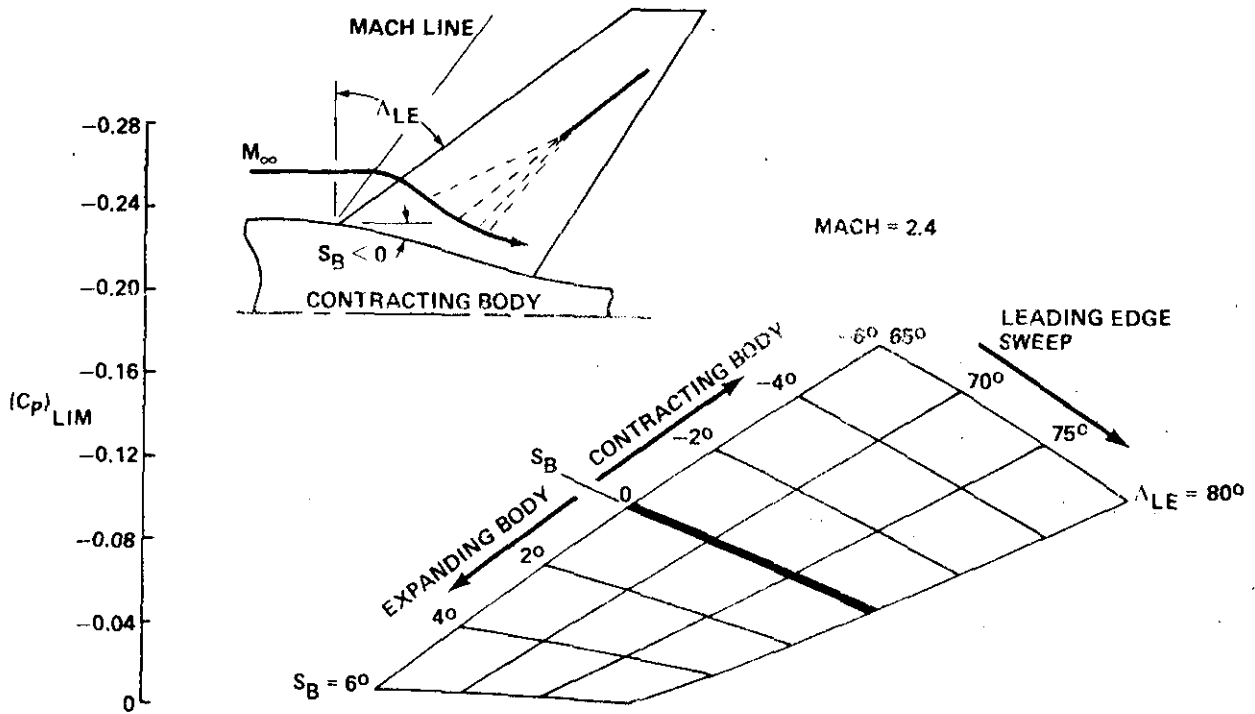
Figure 21   Effect of Body Contour on Inboard Shock Criteria
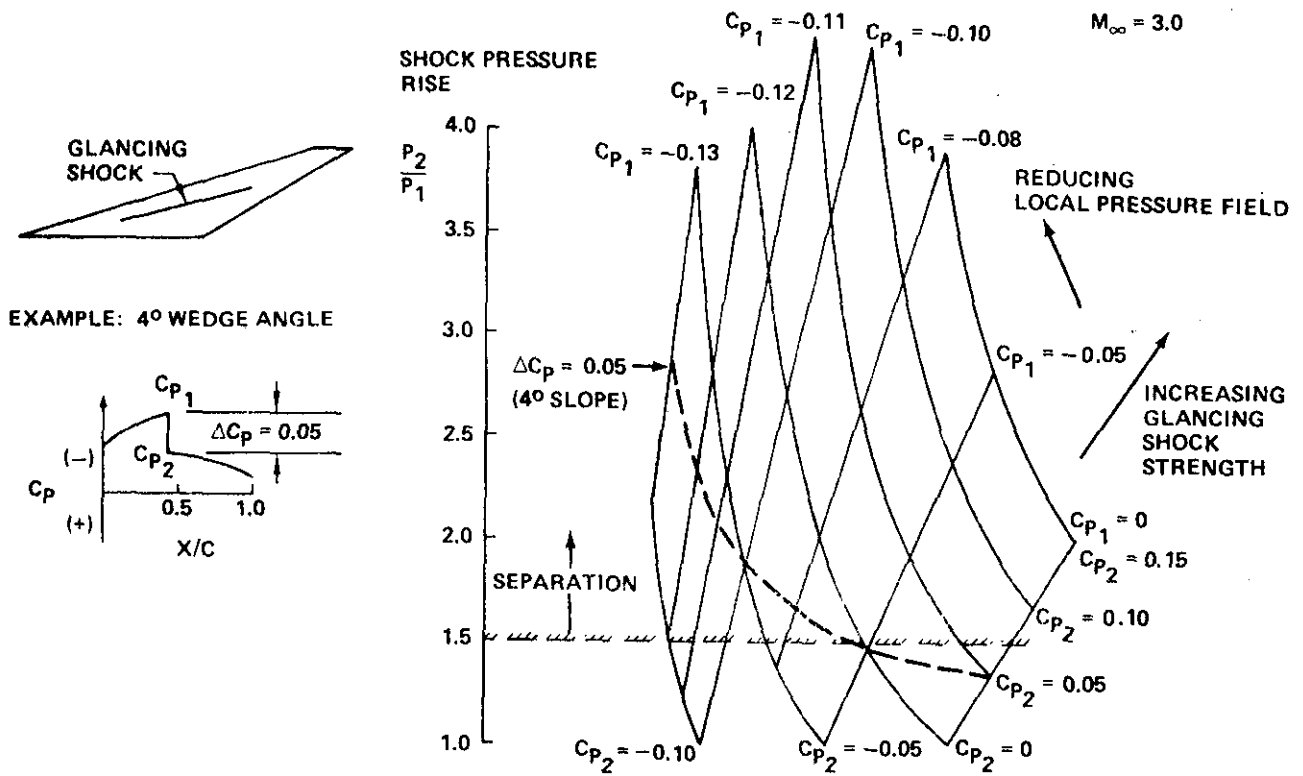
Figure 22   Amplification of Glancing Shock Pressure Rise by Local Pressure Field

- TURBULENT FLOW
- ISENTROPIC FLOW TO TRAILING EDGE
- FREE-STREAM PRESSURE DOWNSTREAM
  OF TRAILING-EDGE SHOCK

BOUNDARY LAYER THICKNESS REYNOLDS NUMBER

1.5×10^4
2.5×10^4
3.5×10^4
4.5×10^4
7.5×10^4

$C_{P_{INCIPIENT\ SEPARATION}}$

$\frac{P_2}{P_1} = 1 + 0.3 M_\ell^2$

MACH NUMBER, M_∞

FREE-STREAM MACH LINE

Λ_{TE}

M_N

TRAILING-EDGE SHOCK

M_∞

P_ℓ P_∞

EFFECT OF SWEEPBACK ON PEAK PRESSURE RATIO

$\frac{P_2}{P_1}$ PEAK

× TWO-DIMENSIONAL DATA
⊙ SWEEP BACK DATA ($M_\infty = 2.36$)

NORMAL MACH NUMBER, M_N

Figure 23   Trailing Edge Shock Separation Criteria

$C_{P_{TE}}$ LIMIT

$0.8\ C_{P_{VAC}}$

0   10°   20°

TRAILING-EDGE SWEEP, Λ_{TE}

30°

40°

INCREASING MACH NUMBER

50°

SONIC TRAILING-EDGE

60°

1.8

INCREASING TRAILING-EDGE SWEEP ANGLE

FREE-STREAM MACH NUMBER, M

Λ_{TE}

SHOCK

M →

C_P (−)

$C_{P_{TE}}$ LIMIT

0.5   1.0

X/C
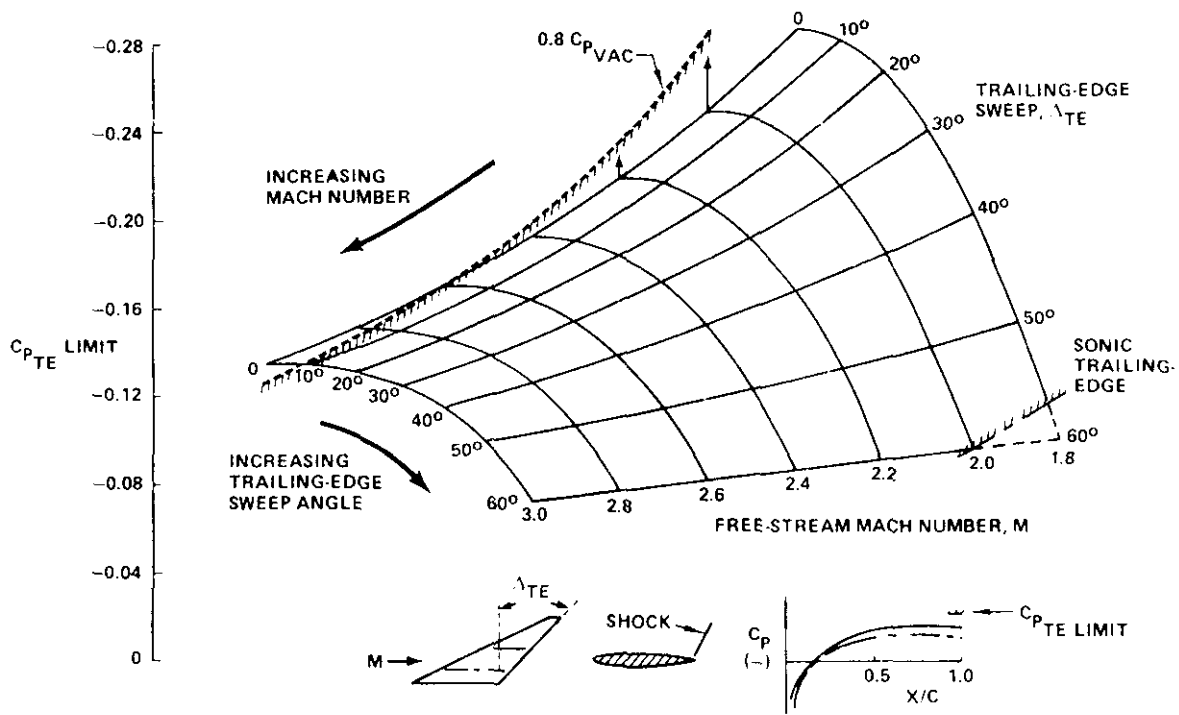
Figure 24   Effect of Trailing Edge Sweep and Mach Number on the Trailing Edge Shock Separation Criteria

INBOARD SHOCK SEPARATION CRITERIA, $\Lambda_{LE} = 75^\circ$

TRAILING-EDGE SHOCK SEPARATION CRITERIA, $\Lambda_{TE} = 61.8^\circ$

$C_{P_{LIMIT}}$

SEPARATED FLOW

0.8 VACUUM

INBOARD SHOCK $C_{P_{LIMIT}}$

ATTACHED FLOW

$\Theta_B = -5^\circ$

$\Theta_B = 0$

MACH NUMBER

$C_{P_{LIMIT}}$

SEPARATED FLOW

0.8 VACUUM LIMIT

ATTACHED FLOW

TRAILING-EDGE LIMITING C_P

MACH NUMBER

75°

TO AVOID TRAILING-EDGE SHOCK SEPARATION

$\Theta_B = -5^\circ$
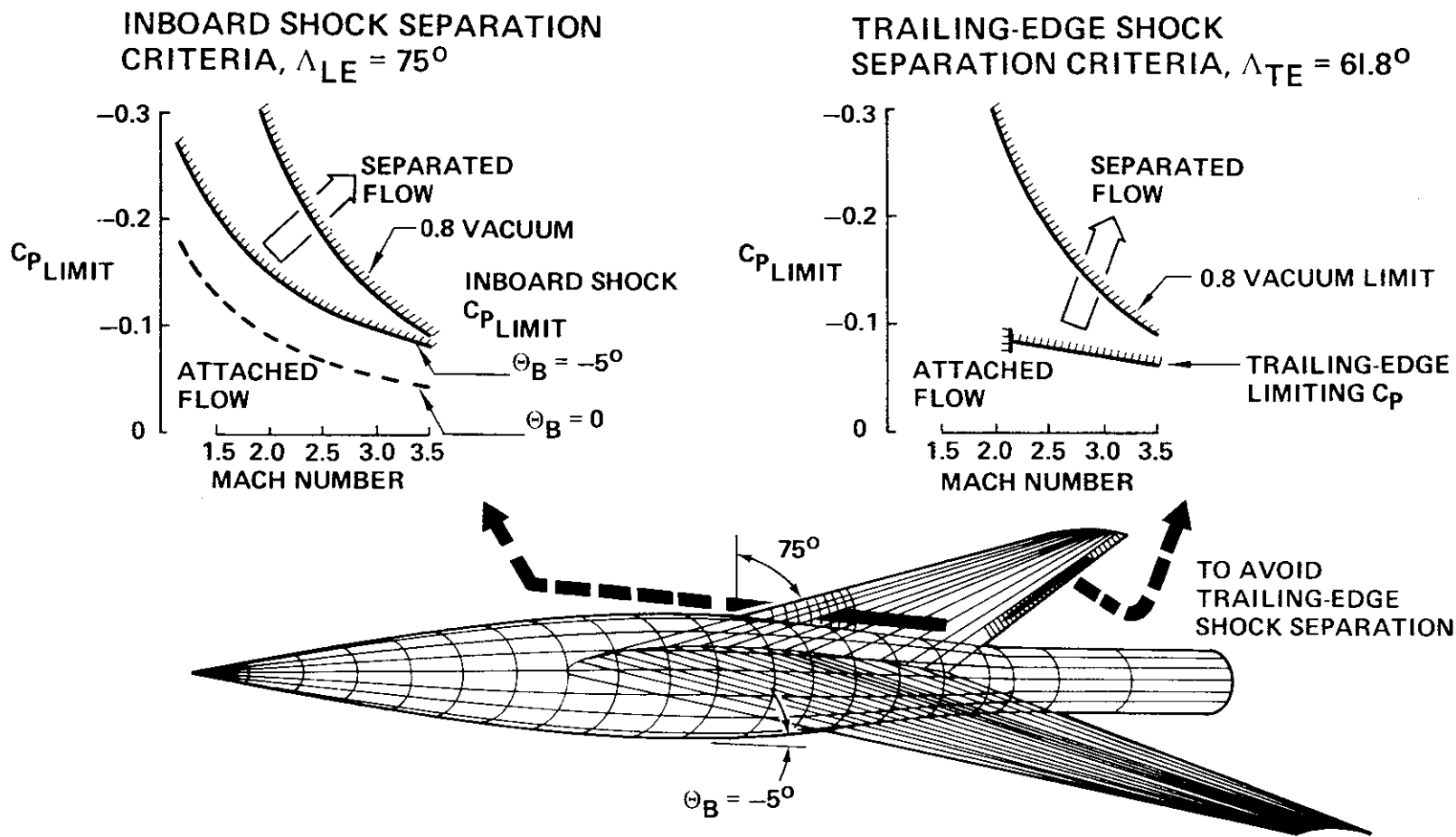
Figure 25   Boeing Wind Tunnel Model Flow Separation Criteria
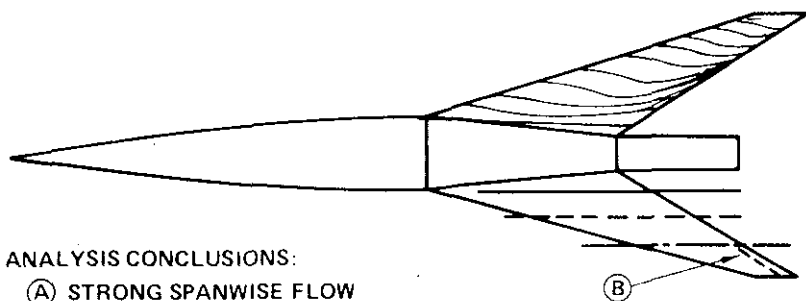
ANALYSIS CONCLUSIONS:

(A) STRONG SPANWISE FLOW

(B) POSSIBLE TRAILING-EDGE SHOCK
SEPARATION OUTBOARD OF 70%
SEMISPAN
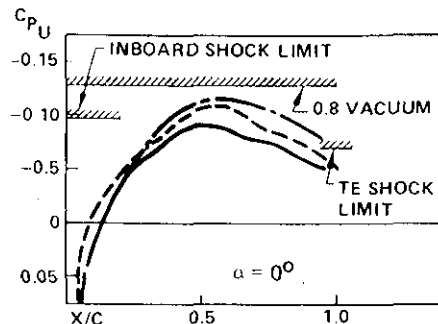
MACH = 3.0	
———	0.3 SEMISPAN
– – –	0.5 SEMISPAN
—·—·	0.7 SEMISPAN
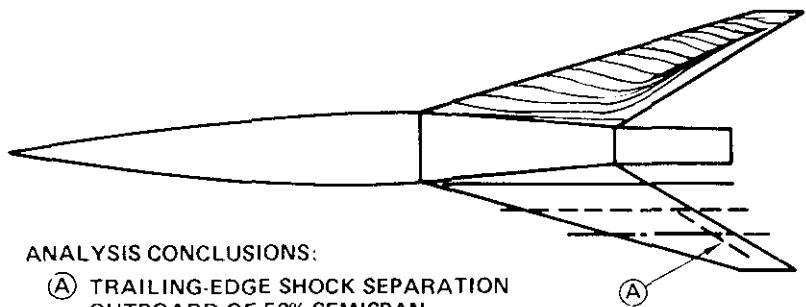
ANALYSIS CONCLUSIONS:

(A) TRAILING-EDGE SHOCK SEPARATION
OUTBOARD OF 50% SEMISPAN
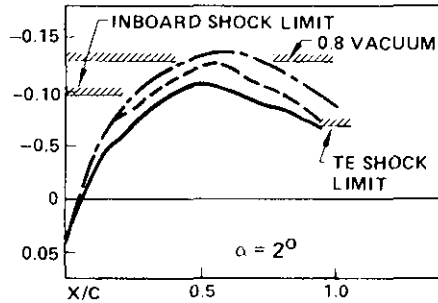
Figure 26A   Comparison of Experimental and Predicted Shock Separation
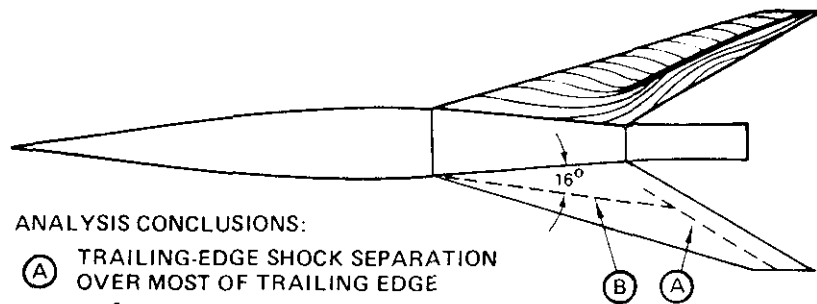
ANALYSIS CONCLUSIONS:

(A) TRAILING-EDGE SHOCK SEPARATION
OVER MOST OF TRAILING EDGE

(B) POSSIBLE INBOARD SHOCK ((-) = 16°)
SEPARATION
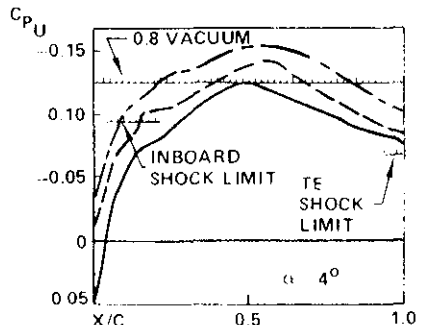
MACH 3.0	
———	0.3 SEMISPAN
– – –	0.5 SEMISPAN
—·—·	0.7 SEMISPAN
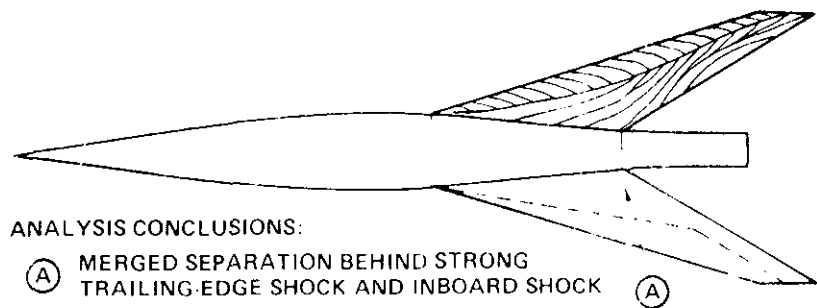
ANALYSIS CONCLUSIONS:

(A) MERGED SEPARATION BEHIND STRONG
TRAILING-EDGE SHOCK AND INBOARD SHOCK
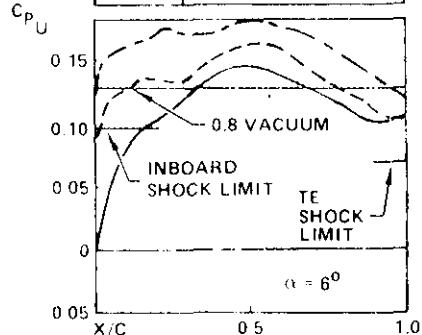
Figure 26B   Comparison of Experimental and Predicted Shock Separation (Concluded)

24

ANGLE OF ATTACK EFFECT ON TRAILING-EDGE PRESSURES

TRAILING-EDGE SEPARATION DEVELOPMENT
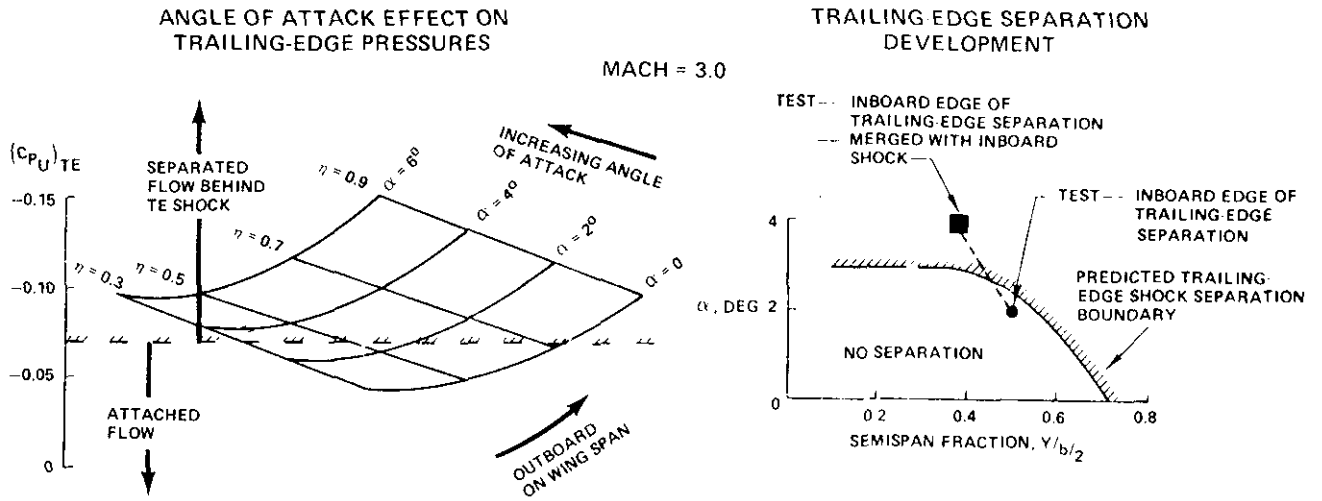
MACH = 3.0

Figure 27   Development of Trailing Edge Shock Separation

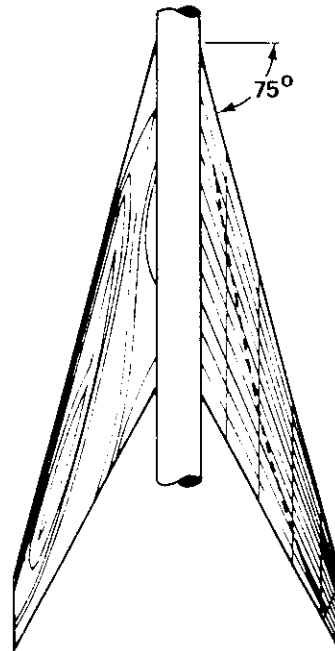## THEORETICAL WING UPPER SURFACE PRESSURES — MACH = 3.0 α = 0°

CURVED MIDBODY ———
CONICAL MIDBODY — — —
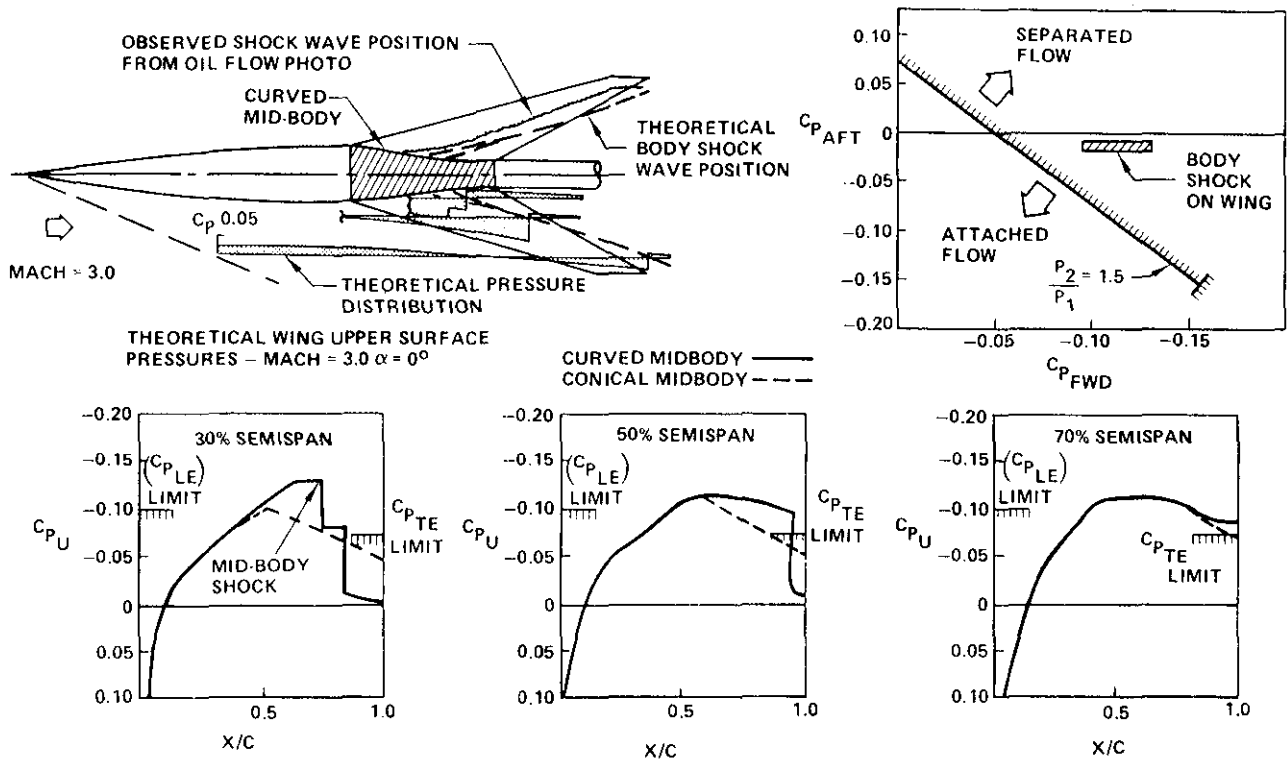
Figure 28   Body Induced Shock Separation
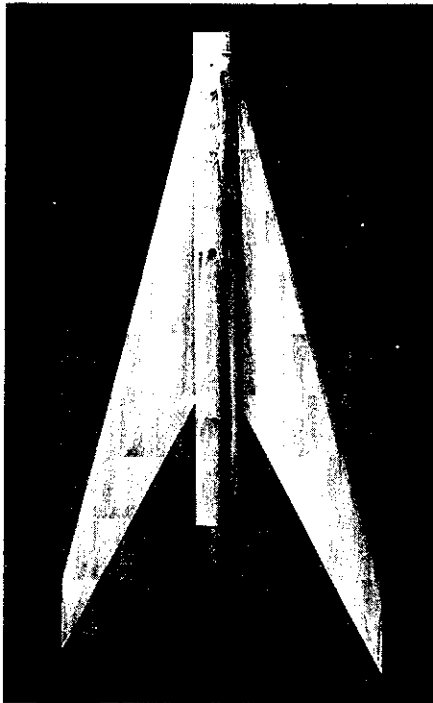
25

OIL FLOW

PRESSURE CONTOUR MAP

THEORETICAL PRESSURES

75°

THEORETICAL UPPER
SURFACE PRESSURES

MACH = 3.0
0.8 VACUUM α = 6.0
LIMIT C_L = 0.10

-0.14
-0.12 $\eta = .9$ TRAILING EDGE
SHOCK LIMIT
-0.10 $\eta = .7$
C_P -0.08 $\eta = .5$
$\eta = .3$
-0.06 SIDE OF BODY
-0.04
-0.02 INBOARD SHOCK LIMIT
0
0.5 1.0
CHORD FRACTION, $X/_C$

MACH = 3.0
α = 6.7°
C_L = 0.112
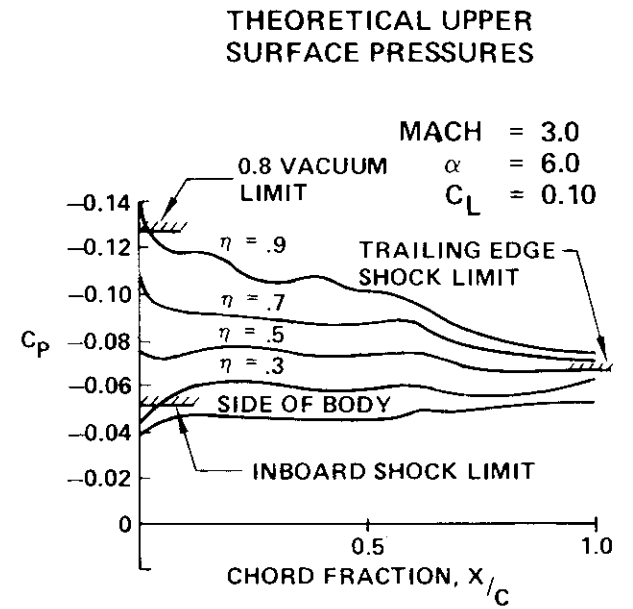
MACH = 3.0
α = 6.3
C_L = 0.105

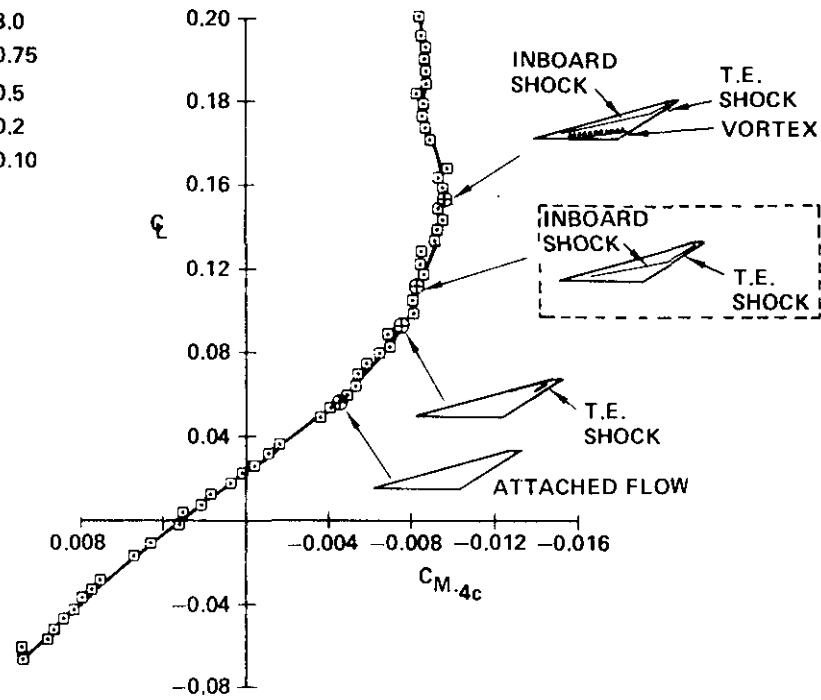*Figure 29   Flow Development on a Mach 3 Uniform Load Wing Upper Surface (Boeing Wind Tunnel Model)*

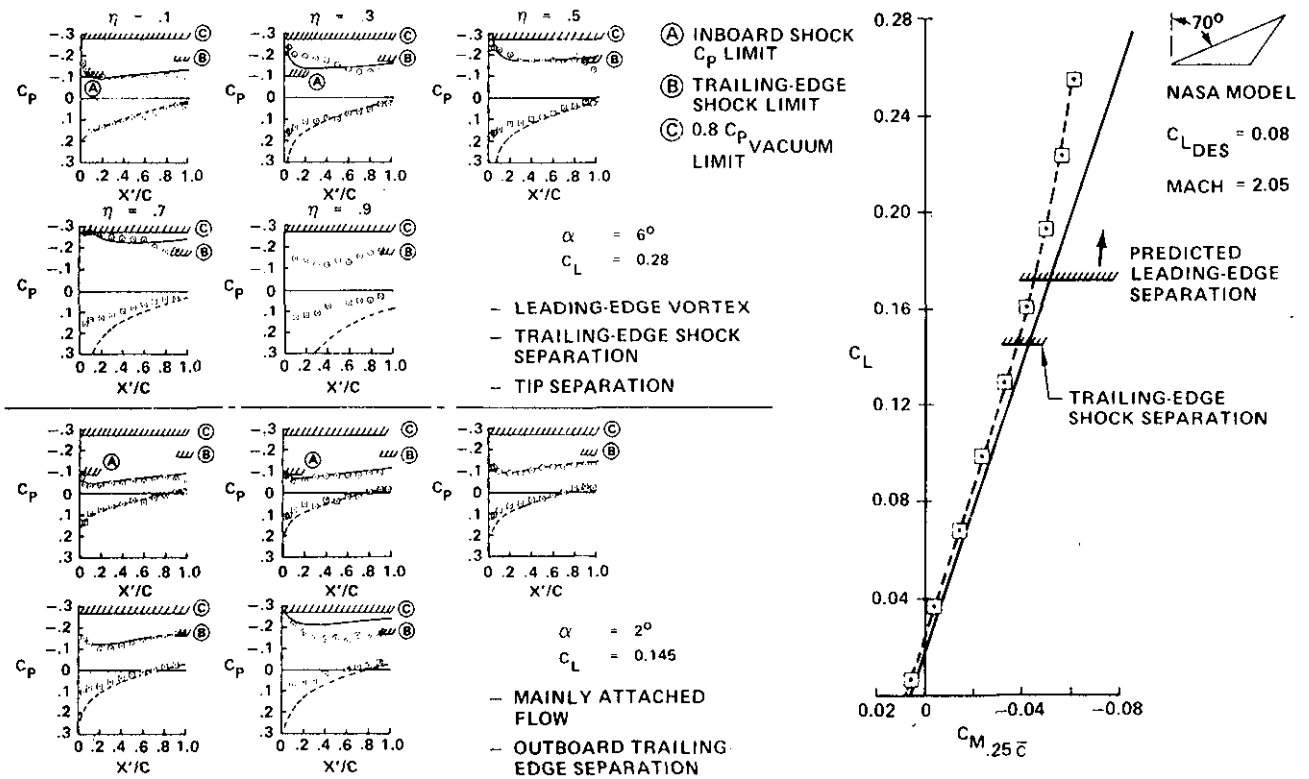Figure 30   Interpretation of Wind Tunnel Force Data (Boeing Wind Tunnel Model)
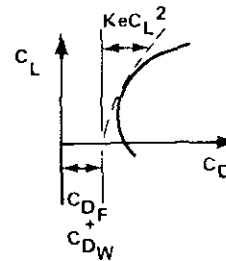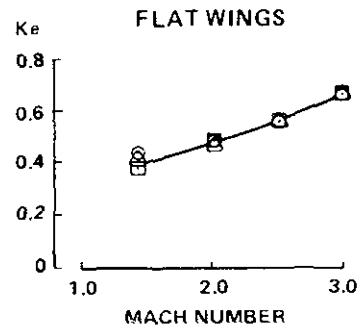

Figure 31   NASA Cambered Wing Pressures and Pitching Moment

27

BOEING TEST DATA	
⊙	2½% BICONVEX
△	5% BICONVEX
⊡	5% MOD 65005

73.8°
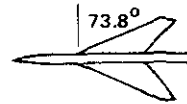
BOEING TEST DATA	
⊙	2½% MOD 65005
△	5% MOD 65005

FLAT WINGS

Ke
0.8
0.6
0.4
0.2
0

1.0   2.0   3.0
MACH NUMBER

C_L

KeC_L^2

C_D

$C_{D_F} + C_{D_W}$

THEORETICAL C_P UPPER	
M = 3.0 C_L = 0.10	
-----	30% SEMISPAN
——	50% SEMISPAN
—·—	80% SEMISPAN

CAMBERED & TWISTED WINGS

Ke
0.8
0.6
0.4
0.2
0

t/c = 5%

t/c = 2½%

1.0   2.0   3.0
MACH NUMBER

t/c = 2.5%

C_{P_U}
TE SHOCK LIMIT
0.8 VACUUM
-0.15
-0.10
-0.05
0
INBOARD SHOCK LIMIT
0.05
0.5   1.0
X/C

t/c = 5%

C_{P_U}
TE SHOCK LIMIT
0.8 VACUUM
-0.15
-0.10
-0.05
0
INBOARD SHOCK LIMIT
0.05
0.5   1.0
X/C

t/c = 2.5%

C_{P_U}
TE SHOCK LIMIT
0.8 VACUUM
-0.15
-0.10
-0.05
0
FORWARD SHOCK LIMIT
0.05
0.5   1.0
X/C

t/c = 5%

C_{P_U}
TE SHOCK LIMIT
0.8 VACUUM
-0.15
-0.10
-0.05
0
FORWARD SHOCK LIMIT
0.05
0.5   1.0
X/C

Figure 32   Wing Thickness Effect on Drag Due to Lift

AVOID FRONT SHOCK

$C_{P_{LIMIT}}$

CRITERION2
WING WITH M = 1.4 OPTIMUM BODY
WING WITH NONCONTOURED BODY
$\Lambda_{LE} = 45^o$

-0.4

-0.2

1.0   1.5   2.0
MACH NUMBER

C_P > CRITERION1

C_P > CRITERION2
AVOID BOUNDARY
LAYER SEPARATION

C_P > CRITERION3
AVOID TRAILING-EDGE SEPARATION
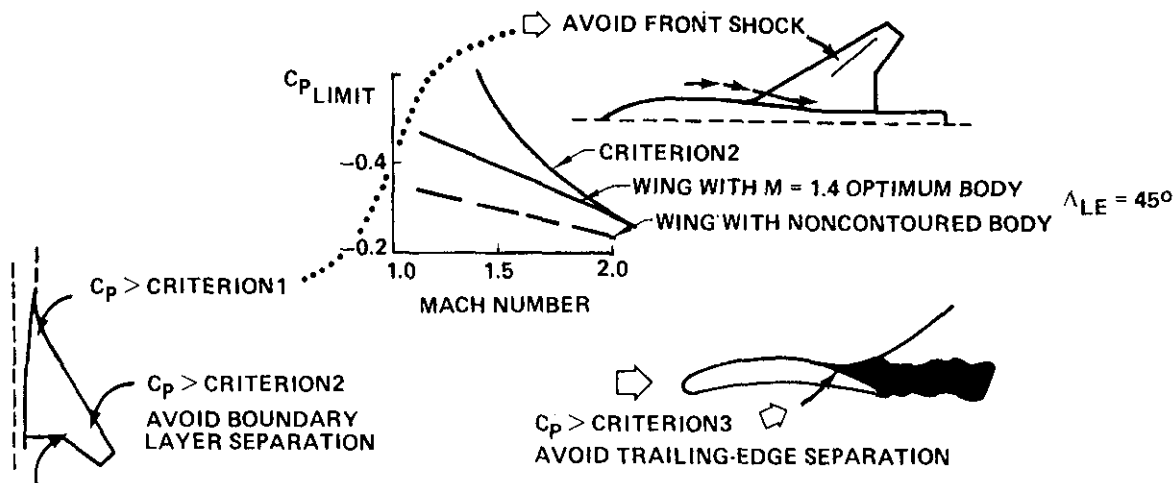
DESIGN PROCEDURE

1. CALCULATE WING UPPER SURFACE
   PRESSURE DISTRIBUTIONS AT THE
   DESIGN CONDITION

2. COMPARE C_P WITH CRITERIA

3. IF C_P SATISFIES CRITERIA, THEN
   SEPARATION WILL NOT OCCUR,
   OTHERWISE THE DESIGN MUST BE
   MODIFIED

$C_{P_{LIMIT}}$

CRITERION2
$\Lambda_{TE} \approx 0^o$
$\Lambda_{TE} = 16^o$

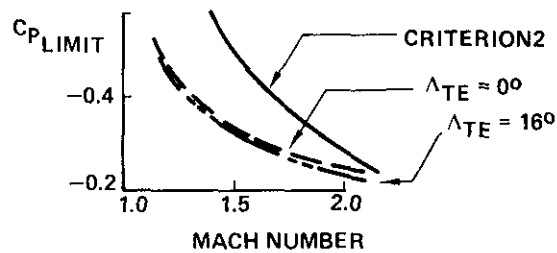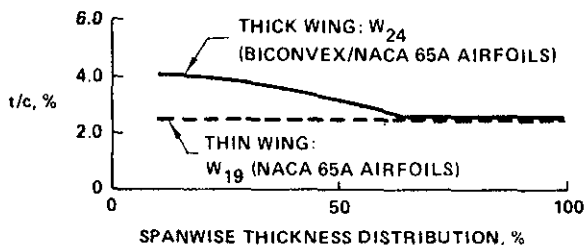-0.4

-0.2

1.0   1.5   2.0
MACH NUMBER

Figure 33   Supersonic Wing Design Criteria

SWEEP = 75°
MACH = 3.0

6.0

4.0

t/c, %

2.0

0

THICK WING: W_{24}
(BICONVEX/NACA 65A AIRFOILS)

THIN WING:
W_{19} (NACA 65A AIRFOILS)

0   50   100
SPANWISE THICKNESS DISTRIBUTION, %

$-C_P$
$-C_P$
80% SPAN
20% SPAN

THEORETICAL UPPER SURFACE PRESSURE
DISTRIBUTION AT MACH = 3.0, C_L = 0.1

0.006

0.004

ΔC_D

0.002

0

⊙	C_L = 0
⊡	C_L = 0.05
△	C_L = 0.15

ΔC_{D_W}

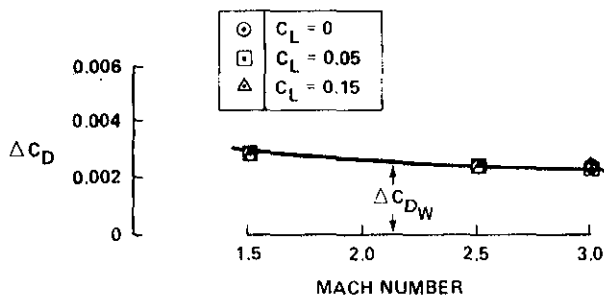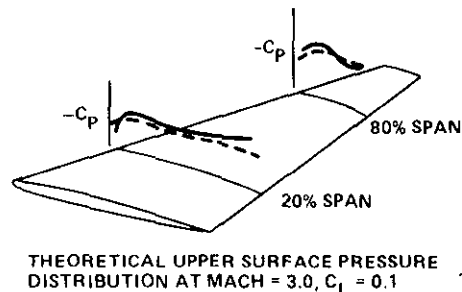1.5   2.0   2.5   3.0
MACH NUMBER

C_L

W_{19} W_{24}
ΔC_D

C_D
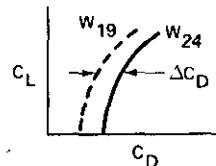
Figure 34   Tailored Wing Thickness Distribution

SST WING

DRAG DUE TO LIFT

FLAT WING

SST WING DESIGN

DRAG
DUE TO
LIFT

OPTIMUM

MACH NUMBER

B-B
TIP
t/c (MAX) = 2.4%

A-A
SIDE OF BODY
t/c (MAX) = 3.2%

TWIST 3.6°
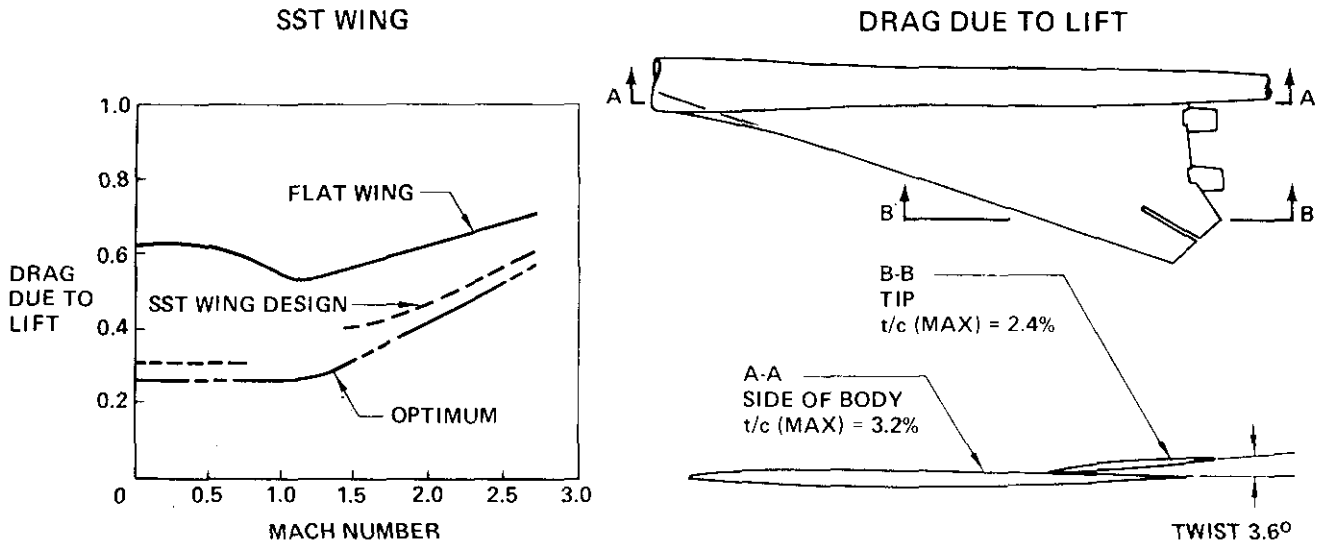
Figure 35   Early U.S. SST Wing Design Success

LEADING-EDGE
SEPARATION

MANEUVER
CONDITION

SEPARATION BEHIND
INBOARD SHOCK

SEPARATION BEHIND
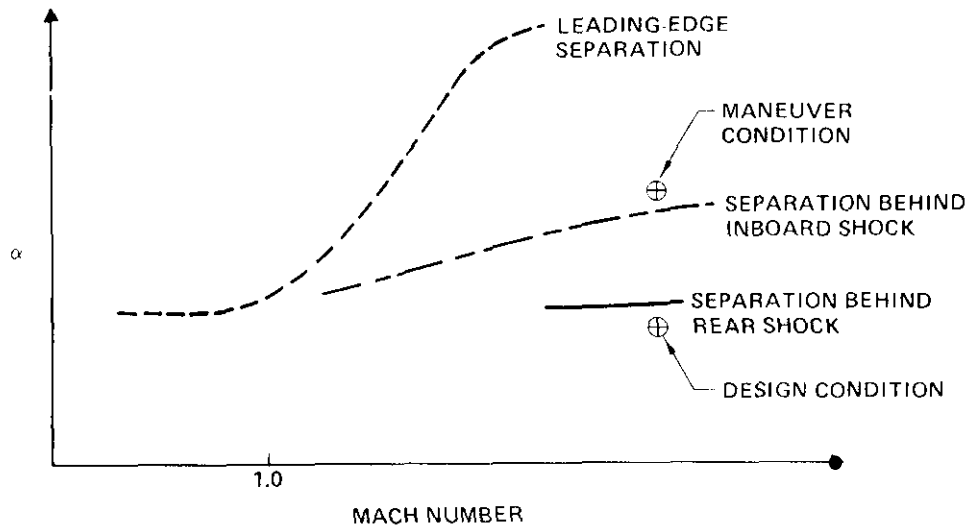REAR SHOCK

DESIGN CONDITION

α

MACH NUMBER

Figure 36   Typical Flow Development Boundaries for a Highly Swept Arrow Wing

30